

Orbital liquid in the e_g orbital Hubbard model in $d = \infty$ dimensions

Louis Felix Feiner

Institute for Theoretical Physics, Utrecht University, PO Box 80.000, 3508 TA Utrecht, Netherlands

Andrzej M. Oleś 

*Max Planck Institute for Solid State Research, Heisenbergstrasse 1, D-70569 Stuttgart, Germany
and Institute of Theoretical Physics, Jagiellonian University, Prof. Stanisława Łojasiewicza 11, PL-30348 Kraków, Poland*



(Received 11 June 2022; revised 31 October 2022; accepted 3 November 2022; published 28 November 2022)

We demonstrate that the three-dimensional e_g orbital Hubbard model can be generalized to arbitrary dimension d , and that the form of the result is determined uniquely by the requirements that (i) the twofold degeneracy of the e_g orbital be retained, and (ii) the cubic lattice be turned into a hypercubic lattice. While the local Coulomb interaction U is invariant for each basis of orthogonal orbitals, the form of the kinetic energy depends on the orbital basis and takes the most symmetric form for the so-called complex-orbital basis. Characteristically, with respect to this basis, the model has two hopping channels: one that is orbital-flavor conserving, and a second one that is orbital-flavor nonconserving. We show that the noninteracting electronic structure consists of two nondegenerate bands of plane-wave real-orbital single-particle states for which the orbital depends on the wave vector. Due to the latter feature each band is unpolarized at any filling, and has a non-Gaussian density of states at $d = \infty$. The *orbital liquid* state is obtained by filling these two bands up to the same Fermi energy. We investigate the e_g orbital Hubbard model in the limit $d \rightarrow \infty$, treating the on-site Coulomb interaction U within the Gutzwiller approximation, thus determining the correlation energy of the orbital liquid and the (disordered) paraorbital states. In perfect analogy with the case of the spin Hubbard model, the Gutzwiller approximation is demonstrated to be exact at $d = \infty$ for the orbital Hubbard model, because of the collapse of electron correlations to a single site. At half-filling (one electron per site on average, $n = 1$) one finds a Brinkman-Rice type “metal-insulator” transition in the orbital liquid, which is analogous to the transition for a paramagnetic state in the spin model, but occurs at stronger Hubbard interaction U due to the enhanced kinetic energy provided by the nonconserving hopping channel. We show that the orbital liquid is the ground state everywhere in the (n, U) phase diagram except close to half-filling at sufficiently large U , where ferro-orbital order with real orbitals occupied is favored. The latter feature is shown to be specific for $d = \infty$, being of mathematical nature due to the exponential tails in the density of states.

DOI: [10.1103/PhysRevResearch.4.043134](https://doi.org/10.1103/PhysRevResearch.4.043134)

I. INTRODUCTION

Our understanding of electron correlations in solids stems to a considerable extent from the Hubbard model [1]. This describes electrons which propagate on a lattice and interact by an on-site Coulomb interaction U when two electrons with opposite spins occupy the same site. At half-filling (one electron per site) it provides a picture of a metal-insulator transition due to electron localization and of magnetism caused by superexchange according to ideas going back to Anderson [2]. Away from half-filling it represents the competition between the kinetic energy of the electrons and the localizing effect of the Coulomb interaction. An important development regard-

ing the Hubbard model was the discovery by Metzner and Vollhardt that in the limit of infinite dimension ($d = \infty$) only the on-site correlations survive [3,4]. They thus proved that in this limit the Gutzwiller approximation to the variational ground state wave function [5–7] becomes exact [8], and that a similar property applies [9] to the resonating valence-bond (RVB) state [10]. It was then shown that the ground state phase diagram of the doped Hubbard model at $d = \infty$ includes ferromagnetic (FM) and antiferromagnetic (AF) order stabilized at large Coulomb interaction [11].

The e_g orbital Hubbard model [12–16], discussed in the present paper, describes spinless fermions which propagate on a lattice of atoms with twofold degenerate orbitals and which interact by an on-site Coulomb interaction U when two electrons occupy both orbitals on a site. Importantly, the hopping strength t is dependent on the orientation of the orbitals with respect to the hopping direction. Obviously, with twofold orbital degeneracy replacing twofold spin degeneracy, the orbital model closely resembles the spin model, but there is a crucial difference: in the spin model the local symmetry is SU(2) but in the orbital model it is the threefold rotation

Published by the American Physical Society under the terms of the Creative Commons Attribution 4.0 International license. Further distribution of this work must maintain attribution to the author(s) and the published article's title, journal citation, and DOI. Open access publication funded by the Max Planck Society.

group C_3 , and moreover this is linked to the hopping. As an immediate consequence the model contains, in addition to the familiar orbital-conserving hopping channel [analogous to the spin-conserving hopping channel in the (spin) Hubbard model], also an orbital-flipping hopping channel. This leads in the three-dimensional (3D) case to the existence of an orbital liquid (OL) state [12,13], in analogy to a spin liquid [17,18], which is disordered in a way different from paramagnetism. Our aim is to analyze the limit $d \rightarrow \infty$ along the lines set out by Metzner and Vollhardt and explore whether this gives further insight into the properties of the e_g orbital Hubbard model and the OL state in particular.

The e_g orbital Hubbard model comes from the field of spin-orbital physics, which has developed over the last two decades into a very active and challenging part of solid state physics which unifies frustrated magnetism and the phenomena in strongly correlated electron systems. It arose from the pioneering ideas of Kugel and Khomskii [19] who recognized that, in transition metal oxides with partly filled degenerate $3d$ orbitals, both the spin and the orbital degrees of freedom are quantum variables and have to be treated on equal footing. At large local Coulomb interaction U most of these compounds are Mott (or charge-transfer) insulators due to electron localization, and superexchange arises from coupled spins and orbitals together [20–22]. More recently similar phenomena have been found in ultracold fermion systems in optical lattices [23].

In the degenerate-orbital case [24], quantum fluctuations in the insulating state are enhanced with respect to the nondegenerate case [25–27]. In some cases these joint fluctuations could even trigger a new state of quantum matter: a spin-orbital liquid in model [28] or real systems [29–31]. In most cases, however, one finds spin-orbital order due to spin interactions of a Heisenberg form with $SU(2)$ symmetry, coupled to anisotropic orbital superexchange [32–51], in agreement with the Goodenough-Kanamori rules [52]. These interactions give in general entangled ground states [53–58]. We remark that the physical properties of such systems are very rich and depend on whether the orbital degrees of freedom are of e_g , t_{2g} , or p type. The main difference is the spatial character of the orbitals which makes their interactions directional.

An issue of high interest is how such systems, characterized by the presence of orbital and spin degrees of freedom, behave under doping, i.e., how their properties compare with the more familiar behavior of doped spin systems, such as the high- T_c cuprates [59–61]. In the latter systems remarkable progress has been achieved by employing dynamical mean-field theory (DMFT) [62], which gave very valuable insights into the transport properties [63] and spectral functions [64]. This theory, which is currently used widely for electronic structure calculations of strongly correlated materials where the one-electron description breaks down [65], is in fact based on the above-mentioned discovery by Metzner and Vollhardt regarding the Hubbard model [3,4].

A realistic description of transition metal oxides with degenerate $3d$ orbitals requires the treatment of spin-orbital physics in at least a degenerate Hubbard model, involving both orbital and spin degrees of freedom [22]. However, in particular situations the problem becomes somewhat simplified. In spin-orbital systems with FM order and weak spin-orbit

coupling, the spins may be ignored because the spin flavor is conserved in the hopping processes, and the spins disentangle from the orbitals [66,67] and do not contribute to the dynamics. The degenerate Hubbard model appropriate for the spin-orbital system [68] then reduces to an orbital Hubbard model with direction-dependent hopping.

When the active orbitals are of t_{2g} type this orbital Hubbard model is rather similar to the standard spin Hubbard model because the orbital flavor is then conserved in the hopping processes (like for spin) but the hopping is two-dimensional (2D) [29,69]. This gives almost localized orbital polarons for single holes [70,71] or orbital stripes due to self-organization of the doped Mott insulator [72,73].

However, in doped FM systems with active e_g orbitals [74,75] the orbital flavor is not conserved, in contrast to the t_{2g} case above, and the kinetic energy consists of all possible hopping processes including those which change the orbital flavor. Obviously, this represents a qualitative difference with the spin Hubbard model. Moreover, it suggests that disordered phases are favored more in doped e_g than in doped t_{2g} systems.

In doped manganites the FM metallic phase occurs due to the kinetic energy gain by the double exchange mechanism [76], because antiferromagnetic (AF) bonds hinder electron hopping while hopping is unrenormalized along FM bonds, and the e_g electrons reorient the t_{2g} spins coupled to them by Hund's rule exchange. Double exchange for strongly correlated e_g electrons is indeed responsible for the spectacular properties of doped perovskite manganites [77–79], including colossal magnetoresistance in the FM metallic phase [80]. At low doping the A-type AF order in $\text{La}_{1-x}\text{Sr}_x\text{MnO}_3$ favors e_g electron transport within 2D (a, b) planes, and gradually changes the spin order to FM along the c axis. Increasing doping generates orbital polarons [81]. Already a single polaron triggers [82] an insulator-to-metal transition that occurs here to a FM metallic phase. Eventually, the orbitals decouple from the spins and a disordered orbital liquid (OL) phase arises in a 3D system [12–15]. This OL phase may explain the cubic dispersion relation of magnons in the FM phase of some manganites, which indicates that magnetic interactions are isotropic [83,84] unless they couple strongly to orbital excitations [57]. Specifically this compound, $\text{La}_{1-x}\text{Sr}_x\text{MnO}_3$, provides a prime example of the physical situation represented by the orbital model studied in this paper, with the spins integrated out and the dynamics determined solely by the orbitals.

So the e_g orbital Hubbard model, while still directly relevant for a class of doped FM insulators, is the *simplest nontrivial multiorbital model representing interacting lattice fermions*, and as such presents an opportunity for studying fundamental issues in orbital dynamics. Moreover, because of their mathematical similarity one can readily compare its behavior with that of the (spin) Hubbard model, at the same time exploiting the wealth of results available for the latter one.

As stated, our overall aim is to investigate whether the limit of infinite dimension elucidates the characteristic features of the e_g orbital Hubbard model, like it does for the spin Hubbard model [11]. In particular we want to establish which features found in the 3D case [12–15] are characteristic for the model as such, i.e., continue to hold for arbitrary dimension up to $d = \infty$, and which are specific for $d = 3$ *per se* or are caused

by the fact that at finite dimension the Gutzwiller approach is an approximation.

The purpose of this paper is therefore

(i) to derive the orbital e_g model at arbitrary dimension d from the requirements that the twofold degeneracy of the e_g orbitals be retained and that the cubic lattice symmetry be turned into a hypercubic symmetry;

(ii) to highlight the fundamental difference with the spin Hubbard model, which is that the orbital flavor is not conserved and the kinetic energy is therefore potentially larger, which should hinder orbital order and favor states with disordered orbitals;

(iii) to demonstrate that the Gutzwiller approximation is again exact in the limit $d \rightarrow \infty$ like it is for the (spin) Hubbard model;

and next to investigate

(iv) in what way the OL state avoids orbital polarization, and the role played therein by symmetry;

(v) whether at half-filling electron localization induces a metal-insulator transition in the OL state and, if so, at which critical value of the on-site interaction U ;

(vi) what the nature is of the ground state (long-range order of ferro type or alternating type, or rather disordered of paraorbital type or orbital-liquid type), dependent on the strength of the interaction U and the particle density n .

The paper is organized as follows. In Sec. II A we introduce the orbital Hubbard model for spin-polarized e_g electrons for a cubic lattice ($d = 3$), and discuss its symmetry properties. We show that the cubic symmetry of the hopping may be better appreciated when a particular basis consisting of two orbitals with complex coefficients is used. This serves to introduce the orbital model at general dimension d and at $d = \infty$ in Sec. II B. Next we use the translational invariance to present the noninteracting Hamiltonian in momentum space in Sec. II C. Band dispersion and densities of states for complex and real single-particle states are presented in Secs. III A and III B, respectively. In Sec. III C we address the single-particle eigenstates and show that they exhibit a generic splitting into a lower and an upper band. The orbital model is compared at dimension $d = \infty$ with the spin model in Sec. III D and we argue from the densities of states that its general feature is an enhanced kinetic energy. In Sec. III E we analyze the kinetic energy in dependence of filling and compare it for the simplest symmetry-broken states, disordered (paraorbital) states, and the OL state built from the single-particle eigenstates.

The electron correlations are described using the Gutzwiller approximation within a generalization of the Metzner approach [8,9], analyzed in Sec. IV A, and we evaluate the renormalized propagator at $d = \infty$ using the collapse of diagrams to a single site in Sec. IV B. The general formalism for uniform and two-sublattice states is introduced in Sec. IV C. In Sec. V we treat specific trial variational states: (i) ordered states in Sec. V A and (ii) the OL phase in Sec. V B, concluding the demonstration that the Metzner approach remains valid in the orbital case. In Sec. VI we compare the OL in the orbital Hubbard model with the paramagnet in the spin Hubbard model, and show that a Brinkman-Rice transition takes place in the OL just like in the paramagnet but for a considerably larger value of U . The results of the numerical analysis and the phase diagram

of the orbital Hubbard model at $d = \infty$ are presented in Sec. VII. At the end we focus on some general aspects of the orbital physics and suggest possible extensions of the present study (Sec. VIII A). The paper is concluded in Sec. VIII B by pointing out the differences between the spin and orbital Hubbard model in infinite dimension. In the Appendix we present a proof that the orbital liquid phase is unpolarized.

II. THE e_g ORBITAL HUBBARD MODEL

A. The model at dimension $d = 3$

The usual choice of basis for e_g orbitals in a 3D cubic lattice is to take

$$|z\rangle \equiv \frac{1}{\sqrt{6}}(2z^2 - x^2 - y^2), \quad |\bar{z}\rangle \equiv \frac{1}{\sqrt{2}}(x^2 - y^2), \quad (2.1)$$

called *real orbitals*. However, because this basis is the natural one only for the bonds parallel to the c axis but not for those in the (a, b) plane, the kinetic energy takes then a rather nonsymmetric form, having a very different appearance depending on the bond direction. It is thus preferred to use instead the basis of *complex orbitals* at each site [85],

$$|+\rangle = \frac{1}{\sqrt{2}}(|z\rangle + i|\bar{z}\rangle), \quad |-\rangle = \frac{1}{\sqrt{2}}(|z\rangle - i|\bar{z}\rangle), \quad (2.2)$$

corresponding to “up” and “down” pseudospin flavors, with the local pseudospin operators defined as

$$\hat{T}_i^+ = \hat{c}_{i+}^\dagger \hat{c}_{i-}, \quad \hat{T}_i^- = \hat{c}_{i-}^\dagger \hat{c}_{i+}, \\ \hat{T}_i^z = \frac{1}{2}(\hat{c}_{i+}^\dagger \hat{c}_{i+} - \hat{c}_{i-}^\dagger \hat{c}_{i-}) = \frac{1}{2}(\hat{n}_{i+} - \hat{n}_{i-}). \quad (2.3)$$

For later reference it is convenient to introduce also electron creation operators $\hat{c}_i^\dagger(\psi_i, \theta_i)$ which create e_g electrons in orbital coherent states $|\Omega_i\rangle \equiv |\Omega_i(\psi_i, \theta_i)\rangle$ at site i , defined as

$$|\Omega_i\rangle \equiv e^{-i\theta_i/2} \cos\left(\frac{\psi_i}{2}\right)|i+\rangle + e^{+i\theta_i/2} \sin\left(\frac{\psi_i}{2}\right)|i-\rangle, \quad (2.4)$$

in analogy with the well-known spin coherent states [86]. The local pseudospin operator in this state is

$$\langle \Omega_i | \hat{T}_i | \Omega_i \rangle = \frac{1}{2}(\sin \psi_i \cos \theta_i, \sin \psi_i \sin \theta_i, \cos \psi_i), \quad (2.5)$$

i.e., it behaves like a vector [87].

The parameter space of the coherent orbital (2.4) is a sphere, with the “poles” ($\psi_i = 0$ and $\psi_i = \pi$) corresponding to the complex orbitals $|i+\rangle$ and $|i-\rangle$, and the “equator” ($\psi_i = \pi/2$) corresponding to (linear combinations of) the real orbitals,

$$\left| \Omega_i\left(\frac{\pi}{2}, \theta_i\right) \right\rangle = \cos\left(\frac{\theta_i}{2}\right)|iz\rangle + \sin\left(\frac{\theta_i}{2}\right)|i\bar{z}\rangle. \quad (2.6)$$

The three real bases, $\{|ix\rangle, |i\bar{x}\rangle\}$, $\{|iy\rangle, |i\bar{y}\rangle\}$, and $\{|iz\rangle, |i\bar{z}\rangle\}$, associated with the cubic axes a , b , and c , respectively, are obtained by setting the in-plane angle $\theta_i/2$ equal to $\chi_a/2 = +2\pi/3$, $\chi_b/2 = -2\pi/3$, and $\chi_c/2 = 0$, for $|ix\rangle$, $|iy\rangle$, and $|iz\rangle$, and to $\chi_\alpha + \pi/2$ ($\alpha = a, b, c$) for $|i\bar{x}\rangle$, $|i\bar{y}\rangle$, $|i\bar{z}\rangle$, as illustrated in Fig. 1(a).

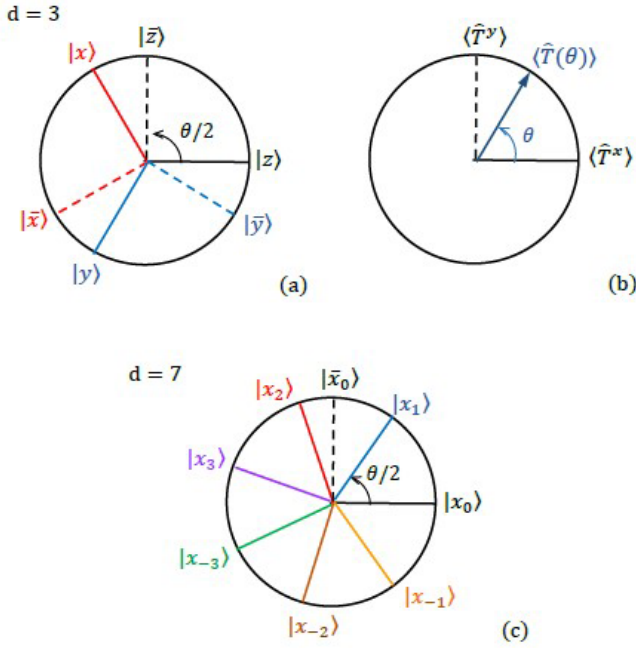


FIG. 1. Schematic representation of the real orbital wave functions in the “equatorial” plane at dimensions (a) $d = 3$, (c) $d = 7$, and (b) of the pseudospin vector at any dimension. The solid lines in (a) correspond to directional $(3z^2 - r^2)$ -like orbitals [the azimuthal angle $\theta_i/2$ in Eq. (2.6) equals one of the $\chi_\alpha/2$], while the dashed lines correspond to the $(x^2 - y^2)$ -like orbitals orthogonal to them ($\theta_i/2$ equaling $\chi_\alpha/2 + \pi/2$). In (c) the solid lines correspond to the $|x_n\rangle_d$ orbitals (the azimuthal angle $\theta_i/2$ equals one of the $\chi_n/2$), while only the dashed line corresponding to the central orthogonal orbital $|\bar{x}_0\rangle_d$ is shown.

In the complex-orbital representation the *orbital Hubbard model* for e_g electrons in $d = 3$ takes the form [13]

$$\mathcal{H}_3 = -\frac{1}{2} t \sum_{(ij) \parallel \hat{\alpha}} \{(\hat{c}_{i+}^\dagger \hat{c}_{j+} + \hat{c}_{i-}^\dagger \hat{c}_{j-}) + \gamma(e^{-i\chi_\alpha} \hat{c}_{i+}^\dagger \hat{c}_{j-} + e^{+i\chi_\alpha} \hat{c}_{i-}^\dagger \hat{c}_{j+})\} + U \sum_i \hat{n}_{i+} \hat{n}_{i-}, \quad (2.7)$$

where the parameter γ actually takes the value $\gamma = 1$. This parameter is introduced here as a device by which one may interpolate between the standard two-flavor Hubbard model with hopping $t/2$ at $\gamma = 0$ and the orbital e_g model at $\gamma = 1$. The appearance of the phase factors $e^{\pm i\chi_\alpha}$ is characteristic for the orbital problem; they occur because the orbitals have an actual shape in real space so that each hopping process depends on the bond direction and on the orbitals between which hopping occurs. Moreover, Eq. (2.7) exhibits the crucial feature that (except at $\gamma = 0$) *orbital flavor is not conserved*, or, equivalently, that *pseudospin is not conserved*; compare Eq. (2.3).

The model (2.7) consists of the kinetic energy $H_{\text{kin}} \propto t$ and the interorbital Coulomb interaction $H_{\text{int}} \propto U$. The interaction is invariant under any local basis transformation to a pair of orthogonal orbitals, i.e., it gives an energy U when a double

occupancy occurs in any representation, i.e., either when both real orbitals are simultaneously occupied or when both complex orbitals are occupied,

$$H_{\text{int}} = U \sum_i \hat{n}_{iz} \hat{n}_{i\bar{z}} = U \sum_i \hat{n}_{i+} \hat{n}_{i-}. \quad (2.8)$$

We emphasize that this simple Hubbard-like form of the Coulomb interaction operator obtained here corresponds to the high-spin ($S = 1$) charge excitations, $d_i^1 d_j^1 \rightarrow d_i^2 d_j^2$; these are the only excited states in a FM system. The parameter U stands then for the on-site interorbital Coulomb repulsion, and is in fact lower than the intraorbital Coulomb element (Kanamori parameter) U_0 by $3J_H$ due to Hund’s exchange in the triplet state, i.e., $U = U_0 - 3J_H$ [16,33].

Importantly, as noted in [13], the equivalence of the cubic axes shows up in the kinetic energy term in Eq. (2.7) in a transparent way, viz., as a formal invariance under threefold rotations of the phase angles $\chi_\alpha \mapsto \chi_\alpha - 4\pi/3$ in conjunction with a phase shift of the electron operators $\hat{c}_{i\pm}^\dagger \mapsto e^{\mp 2\pi/3} \hat{c}_{i\pm}^\dagger$. So the relevant symmetry group is C_3 , with the e_g doublets $\{|iz\rangle, |i\bar{z}\rangle\}$ transforming as real E representations, or equivalently the pairs $\{|i+\rangle, |i-\rangle\}$ transforming as conjugate complex A_1 representations.

B. Generalization to large dimension d

This form, Eq. (2.7), therefore lends itself to a natural generalization of the e_g orbital Hubbard model with two orbital flavors $\{|+\rangle, |-\rangle\}$ to large dimension d as follows:

$$\mathcal{H}_d = -\frac{1}{\sqrt{2d}} \frac{t}{2} \sum_{(ij) \parallel \hat{x}_n} \{(\hat{c}_{i+}^\dagger \hat{c}_{j+} + \hat{c}_{i-}^\dagger \hat{c}_{j-}) + \gamma(e^{-i\chi_n} \hat{c}_{i+}^\dagger \hat{c}_{j-} + e^{+i\chi_n} \hat{c}_{i-}^\dagger \hat{c}_{j+})\} + U \sum_i \hat{n}_{i+} \hat{n}_{i-}, \quad (2.9)$$

with $\chi_n = 4\pi n/d$, where $n = -m, -m+1, \dots, m-1, m$, and $d \equiv 2m+1$ (i.e., taken odd for convenience, but d could also be even with only slightly different derivations below), and we note here that $\sum_n e^{i\chi_n} = 0$. So instead of three cubic axes we now have d hypercubic axes $\{\hat{x}_n\}$, labeled by the index n . Importantly, the number of orbital flavors remains 2 (as for spin $S = 1/2$).

The real basis $\{|x_n\rangle_d, |\bar{x}_n\rangle_d\}$ associated with axis \hat{x}_n is given by Eq. (2.6) with $\theta_i/2$ set equal to $\chi_n/2$ and to $\chi_n/2 + \pi/2$, respectively. This is illustrated in Fig. 1(c) for $d = 7$ in comparison with the case for $d = 3$ shown in Fig. 1(a). Figure 1(b) shows the associated behavior of the pseudospin vector, valid both for $d = 3$ and for general d .

The hopping parameter t is scaled in the standard fashion [3,8,11] by $\sqrt{2d}$ in order that the average kinetic energy remains finite as d becomes large. Below we will use the abbreviation $\tilde{t} = t/\sqrt{2d}$ whenever convenient. Again, the parameter γ takes the value $\gamma = 1$ for the orbital problem, in which the orbital flavor (pseudospin) is not conserved, while $\gamma = 0$ for the corresponding spin problem with hopping $t/2$, in which the (spin) flavor is conserved. The interorbital Coulomb interaction $\propto U$ is the same for any dimension d as

it stands for the on-site Coulomb repulsion when both orbital (or spin) flavors are occupied.

Obviously, the equivalence of the hypercubic axes manifests itself in the Hamiltonian \mathcal{H}_d as a d -fold rotational symmetry, i.e., by being invariant under phase shifts $\hat{c}_{i\pm}^\dagger \mapsto e^{\pm i2\pi/d} \hat{c}_{i\pm}^\dagger$ of the electron operators in conjunction with shifts of the angles $\chi_n \mapsto \chi_n - 4\pi/d$, in perfect analogy with the threefold rotational symmetry of \mathcal{H}_3 . So \mathcal{H}_d is invariant under C_d , with the e_g doublets $\{|ix_n\rangle_d, |i\bar{x}_n\rangle_d\}$ still transforming as real E representations. In the limit $d \rightarrow \infty$ the symmetry group C_d turns into $C_\infty \equiv \mathbb{Z}$, which for practical purposes approaches continuous rotational symmetry $U(1)$.

The generalization to dimension $d = 2m + 1$ for the explicit form of the normalized real basis orbitals associated with the central axis \hat{x}_0 in terms of the coordinates x_n is obtained straightforwardly,

$$|x_0\rangle_d \equiv \frac{2}{\sqrt{2d}} \left(\sum_{n=-m}^m \cos(\chi_n/2) x_n^2 \right), \quad (2.10)$$

$$|\bar{x}_0\rangle_d \equiv \frac{2}{\sqrt{2d}} \left(\sum_{n=-m}^m \sin(\chi_n/2) x_n^2 \right), \quad (2.11)$$

of which Eq. (2.1) is seen to be the special case for $d = 3$. We observe that for general dimension d , the ‘‘directional’’ orbital $|x_0\rangle_d$ has a less pronounced directional shape than $|z\rangle = |x_0\rangle_3$ in the 3D case, because of the many finite contributions from all the coordinates x_n with $n \neq 0$, although the square of the central coordinate x_0 still has the largest coefficient. The orthogonal orbital $|\bar{x}_0\rangle_d$ is perpendicular to the \hat{x}_0 axis as in the 3D case (the coefficient of x_0^2 in $|\bar{x}_0\rangle_d$ is zero as $\chi_0 = 0$). When d gets large the shape of $|\bar{x}_0\rangle_d$ resembles that of $|x_0\rangle_d$ but with permuted coordinates [because Eq. (2.11) is obtained by replacing $\chi_n/2$ in Eq. (2.10) by $\chi_n/2 - \pi/2$]. Clearly, at each site all real-orbital basis sets $\{|x_n\rangle_d, |\bar{x}_n\rangle_d\}$ are equivalent. We have made the arbitrary choices to use the set $\{|x_0\rangle_d, |\bar{x}_0\rangle_d\}$ as the reference basis for real orbitals, and for convenience to drop the subscript d .

C. Momentum space representation

Using translational invariance, we introduce creation and annihilation operators in momentum space,

$$\hat{c}_{\mathbf{k}\lambda}^\dagger = \frac{1}{\sqrt{N}} \sum_j e^{i\mathbf{k}R_j} \hat{c}_{j\lambda}^\dagger, \quad (2.12)$$

where λ labels the orbital flavors, e.g., $\{x_0, \bar{x}_0\}$ or $\{+, -\}$, and N is the number of sites. The free-electron part of \mathcal{H}_d , Eq. (2.9), describing the kinetic energy \mathcal{H}_{kin} , may be represented upon Fourier transformation in the form

$$\mathcal{H}_{\text{kin}} = -\tilde{t} \sum_{\mathbf{k}} (\hat{c}_{\mathbf{k}+}^\dagger \hat{c}_{\mathbf{k}-}^\dagger) \begin{pmatrix} A_{\mathbf{k}} & \gamma G_{\mathbf{k}}^* \\ \gamma G_{\mathbf{k}} & A_{\mathbf{k}} \end{pmatrix} \begin{pmatrix} \hat{c}_{\mathbf{k}+} \\ \hat{c}_{\mathbf{k}-} \end{pmatrix}, \quad (2.13)$$

where the dispersion is given by orbital-conserving and orbital-non-conserving terms,

$$A_{\mathbf{k}} = \sum_n \cos k_n, \quad (2.14)$$

$$G_{\mathbf{k}} = \sum_n e^{+i\chi_n} \cos k_n \equiv |G_{\mathbf{k}}| e^{+i\phi_{\mathbf{k}}}. \quad (2.15)$$

It will be convenient to introduce the following definitions,

$$B_{\mathbf{k}} \equiv |G_{\mathbf{k}}| = \left(\sum_{n,n'} \cos(\chi_n - \chi_{n'}) \cos k_n \cos k_{n'} \right)^{1/2}, \quad (2.16)$$

$$C_{\mathbf{k}} \equiv \text{Re}(G_{\mathbf{k}}) = B_{\mathbf{k}} \cos \phi_{\mathbf{k}} = \sum_n \cos \chi_n \cos k_n, \quad (2.17)$$

$$D_{\mathbf{k}} \equiv \text{Im}(G_{\mathbf{k}}) = B_{\mathbf{k}} \sin \phi_{\mathbf{k}} = \sum_n \sin \chi_n \cos k_n. \quad (2.18)$$

One may now absorb the phase factors from the off-diagonal elements of the matrix in Eq. (2.13) into the operators, by defining what we will call ‘‘phased’’ complex-orbital single-particle operators,

$$\hat{c}_{\mathbf{k}\pm}^\dagger = e^{\mp i\phi_{\mathbf{k}}/2} \hat{c}_{\mathbf{k}\pm}^\dagger, \quad (2.19)$$

and rewrite \mathcal{H}_{kin} as

$$\mathcal{H}_{\text{kin}} = -\tilde{t} \sum_{\mathbf{k}} (\hat{c}_{\mathbf{k}+}^\dagger \hat{c}_{\mathbf{k}-}^\dagger) \begin{pmatrix} A_{\mathbf{k}} & \gamma B_{\mathbf{k}} \\ \gamma B_{\mathbf{k}} & A_{\mathbf{k}} \end{pmatrix} \begin{pmatrix} \hat{c}_{\mathbf{k}+} \\ \hat{c}_{\mathbf{k}-} \end{pmatrix}. \quad (2.20)$$

If desired, the kinetic energy may also be rewritten from Eq. (2.13) in terms of the real-orbital operators,

$$\begin{aligned} \mathcal{H}_{\text{kin}} &= -\tilde{t} \sum_{\mathbf{k}} [A_{\mathbf{k}} \hat{A}_{\mathbf{k}} - \gamma (C_{\mathbf{k}} \hat{C}_{\mathbf{k}} + D_{\mathbf{k}} \hat{D}_{\mathbf{k}})] \\ &= -\tilde{t} \sum_{\mathbf{k}} [A_{\mathbf{k}} \hat{A}_{\mathbf{k}} - \gamma B_{\mathbf{k}} (\cos \phi_{\mathbf{k}} \hat{C}_{\mathbf{k}} + \sin \phi_{\mathbf{k}} \hat{D}_{\mathbf{k}})], \end{aligned} \quad (2.21)$$

where

$$\hat{A}_{\mathbf{k}} = (\hat{c}_{\mathbf{k}x_0}^\dagger \hat{c}_{\mathbf{k}x_0} + \hat{c}_{\mathbf{k}\bar{x}_0}^\dagger \hat{c}_{\mathbf{k}\bar{x}_0}), \quad (2.22)$$

$$\hat{C}_{\mathbf{k}} = (\hat{c}_{\mathbf{k}\bar{x}_0}^\dagger \hat{c}_{\mathbf{k}\bar{x}_0} - \hat{c}_{\mathbf{k}x_0}^\dagger \hat{c}_{\mathbf{k}x_0}), \quad (2.23)$$

$$\hat{D}_{\mathbf{k}} = (\hat{c}_{\mathbf{k}x_0}^\dagger \hat{c}_{\mathbf{k}\bar{x}_0} + \hat{c}_{\mathbf{k}\bar{x}_0}^\dagger \hat{c}_{\mathbf{k}x_0}). \quad (2.24)$$

The invariance with respect to the symmetry group C_d of this real-orbital representation of \mathcal{H}_{kin} is warranted by $A_{\mathbf{k}}$ and $\hat{A}_{\mathbf{k}}$ both transforming as A_1 , and by $\{C_{\mathbf{k}}, D_{\mathbf{k}}\}$ and $\{\hat{C}_{\mathbf{k}}, \hat{D}_{\mathbf{k}}\}$ both transforming as real E representations.

We note that whereas the kinetic-energy Hamiltonian (2.13), (2.20), or (2.21) is block-diagonal in \mathbf{k} -space, the orbital flavors $\{+, -\}$ or $\{x_0, \bar{x}_0\}$ are still coupled. The further analysis of the kinetic energy depends on whether some form of symmetry breaking takes place, or whether we deal with an unpolarized orbital state.

III. NONINTERACTING ELECTRONS

Below, in Sec. V, we will calculate the electron correlations due to the on-site Hubbard repulsion U using the type of wave function introduced by Gutzwiller [6,7],

$$|\Psi\rangle = g^{\hat{D}} |\Phi_0\rangle = \prod_i (1 - (1 - g)\hat{D}_i) |\Phi_0\rangle, \quad (3.1)$$

where $|\Phi_0\rangle$ is an arbitrary uncorrelated trial state,

$$\hat{D} = \sum_i \hat{D}_i, \quad \hat{D}_i = \hat{n}_{i+} \hat{n}_{i-}, \quad (3.2)$$

and g is a variational parameter, $0 \leq g \leq 1$. Frequently $|\Phi_0\rangle$ is chosen to be a Gutzwiller wave function proper, i.e., a Fermi-sea state of noninteracting particles,

$$|\Phi_0\rangle = \prod_{\mathbf{k} \in \mathcal{K}_\lambda} \hat{c}_{\mathbf{k}\lambda}^\dagger \prod_{\mathbf{q} \in \mathcal{K}_{\bar{\lambda}}} \hat{c}_{\mathbf{q}\bar{\lambda}}^\dagger |0\rangle, \quad (3.3)$$

where \mathcal{K}_λ and $\mathcal{K}_{\bar{\lambda}}$ are the parts of the d -dimensional Brillouin zone occupied by particles of opposite orbital flavors λ and $\bar{\lambda}$, determined from the condition that the respective single-particle kinetic energies be smaller than Fermi energies $E_{F,\lambda}$ and $E_{F,\bar{\lambda}}$.

For the orbital model, because it has only C_∞ symmetry, even for a Fermi-sea-like $|\Phi_0\rangle$ the free-particle kinetic energy depends on the particular set of orbitals that are occupied, as in the 3D case [13]. This is fundamentally different from the situation for the spin Hubbard model, where because of the SU(2) symmetry of the spins one has just two (spin) flavors quantized along an arbitrary direction in spin space, and both kinetic energy and renormalization depend only on the filling of the spin subbands. Therefore, we analyze in the present section the dispersions and the densities of states (DOSs) for the single-particle states used later on in building variational states $|\Phi_0\rangle$.

A. Complex-orbital single-particle states

Particularly simple is the dispersion for the single-particle states with complex orbitals as defined by Eq. (2.12) for $\lambda = +$ or $\lambda = -$,

$$\varepsilon_+(\mathbf{k}) = \varepsilon_-(\mathbf{k}) \equiv \varepsilon_c(\mathbf{k}) = -\tilde{t} A_{\mathbf{k}}. \quad (3.4)$$

We also consider single-particle states adapted to G-type partitioning of the lattice into A and B sublattices. With the sublattice operators given by

$$\hat{c}_{A\mathbf{k}\lambda}^\dagger = \frac{1}{\sqrt{2}}(\hat{c}_{\mathbf{k}\lambda}^\dagger + \hat{c}_{\mathbf{k}+\mathbf{Q}\lambda}^\dagger), \quad (3.5)$$

$$\hat{c}_{B\mathbf{k}\lambda}^\dagger = \frac{1}{\sqrt{2}}(\hat{c}_{\mathbf{k}\lambda}^\dagger - \hat{c}_{\mathbf{k}+\mathbf{Q}\lambda}^\dagger), \quad (3.6)$$

where $\mathbf{Q} = (\pi, \pi, \dots, \pi)$ and λ is equal to either $+$ or $-$, we introduce single-particle operators with alternating orbitals of opposite flavor λ (on A sites) and $\bar{\lambda}$ (on B sites) according to

$$\hat{c}_{\mathbf{k}\lambda\bar{\lambda},\ell}^\dagger = \frac{1}{\sqrt{2}}(\hat{c}_{A\mathbf{k}\lambda}^\dagger - \hat{c}_{B\mathbf{k}\bar{\lambda}}^\dagger), \quad (3.7)$$

$$\hat{c}_{\mathbf{k}\lambda\bar{\lambda},u}^\dagger = \frac{1}{\sqrt{2}}(\hat{c}_{A\mathbf{k}\lambda}^\dagger + \hat{c}_{B\mathbf{k}\bar{\lambda}}^\dagger). \quad (3.8)$$

From Eq. (2.13) and making use of the relations $A_{\mathbf{k}+\mathbf{Q}} = -A_{\mathbf{k}}$, $B_{\mathbf{k}+\mathbf{Q}} = B_{\mathbf{k}}$, and $\phi_{\mathbf{k}+\mathbf{Q}} = \phi_{\mathbf{k}} + \pi$, one readily finds that they correspond to a lower (ℓ) and an upper (u) band in the (reduced) Brillouin zone, both doubly degenerate, with dispersions given by

$$\begin{aligned} \varepsilon_{+-,\ell}(\mathbf{k}) &= -\varepsilon_{+-,u}(\mathbf{k}) = \varepsilon_{-+,\ell}(\mathbf{k}) = -\varepsilon_{-+,\ell}(\mathbf{k}) \\ &\equiv \varepsilon_{c,\text{ao}}(\mathbf{k}) = -\gamma\tilde{t} C_{\mathbf{k}} = -\gamma\tilde{t} B_{\mathbf{k}} \cos \phi_{\mathbf{k}}, \end{aligned} \quad (3.9)$$

where the first (second) subscript in the first line gives the occupation of the A (B) sublattice. Following the same procedure we also obtain operators for single-particle states with

phased complex orbitals and alternating flavor, and find their dispersions,

$$\begin{aligned} \tilde{\varepsilon}_{+-,\ell}(\mathbf{k}) &= -\tilde{\varepsilon}_{+-,u}(\mathbf{k}) = \tilde{\varepsilon}_{-+,\ell}(\mathbf{k}) = -\tilde{\varepsilon}_{-+,\ell}(\mathbf{k}) \\ &\equiv \tilde{\varepsilon}_{c,\text{ao}}(\mathbf{k}) = -\gamma\tilde{t} B_{\mathbf{k}}. \end{aligned} \quad (3.10)$$

It is noteworthy that the dispersions (3.9) and (3.10) of the two alternating single-particle states are proportional to γ , i.e., they originate entirely from the orbital-flavor nonconserving part of the kinetic energy.

We now proceed to the DOSs associated with the above single-particle states. In the limit $d \rightarrow \infty$ an exact analytical expression can be derived for all single-particle states considered, also for those discussed below. This was well known to be the case for the rather simple dispersion, identical to Eq. (3.4), of the spin Hubbard model [3], but it holds generally because, from a mathematical point of view [88], DOSs are probability distributions and in the limit $d \rightarrow \infty$ are governed by the law of large numbers. It follows that every DOS is either of Gaussian type,

$$\rho(E) = \frac{1}{\sqrt{2\pi}} \frac{1}{wt} e^{-\frac{1}{2}\left(\frac{E}{wt}\right)^2}, \quad (3.11)$$

fully characterized by its (dimensionless) width w , or is derivable fairly simply from Gaussians. For the above dispersions (3.4) and (3.9) the DOSs are Gaussians with widths $w_c = 1/2$ and $w_{c,\text{ao}} = \gamma/2\sqrt{2}$, respectively, while for the dispersion (3.10) one finds that the DOS is a symmetrized Rayleigh distribution [88],

$$\rho_{\tilde{c},\text{ao}}(E) = \frac{2}{\gamma t} \left| \frac{2E}{\gamma t} \right| e^{-\left(\frac{2E}{\gamma t}\right)^2}. \quad (3.12)$$

These three complex-orbital DOSs are shown for the full orbital case, i.e., $\gamma = 1$, in Fig. 2(a) by the blue, green, and purple line, respectively.

B. Real-orbital single-particle states

For the single-particle states with real orbitals as defined by Eq. (2.12) with $\lambda = x_0$ or $\lambda = \bar{x}_0$, and for the single-particle states describing alternating real flavors x_0 and \bar{x}_0 on the sublattices defined in the same way as above by Eqs. (3.5)–(3.8), one finds the dispersions

$$\varepsilon_{x_0}(\mathbf{k}) = -\tilde{t}(A_{\mathbf{k}} + \gamma C_{\mathbf{k}}) \equiv \varepsilon_r(\mathbf{k}), \quad (3.13)$$

$$\varepsilon_{\bar{x}_0}(\mathbf{k}) = -\tilde{t}(A_{\mathbf{k}} - \gamma C_{\mathbf{k}}) \equiv \varepsilon_r(-\mathbf{k}), \quad (3.14)$$

$$\begin{aligned} \varepsilon_{x_0\bar{x}_0,\ell}(\mathbf{k}) &= -\varepsilon_{x_0\bar{x}_0,u}(\mathbf{k}) = \varepsilon_{\bar{x}_0x_0,\ell}(\mathbf{k}) = -\varepsilon_{\bar{x}_0x_0,u}(\mathbf{k}) \\ &\equiv \varepsilon_{r,\text{ao}}(\mathbf{k}) = \gamma\tilde{t} D_{\mathbf{k}} = \gamma\tilde{t} B_{\mathbf{k}} \sin \phi_{\mathbf{k}}. \end{aligned} \quad (3.15)$$

One observes that, as already indicated at the very end of Sec. II B, the sets of real-orbital single-particle states $\{|\mathbf{k}x_0\rangle\}$ and $\{|\mathbf{k}\bar{x}_0\rangle\}$ are equivalent in the limit $d \rightarrow \infty$, in the sense that they have the same energies but at opposite \mathbf{k} . As above for the complex-orbital single-particle states the alternating real-orbital single-particle states correspond to a lower (ℓ) and an upper (u) band in the (reduced) Brillouin zone, both doubly degenerate, and their dispersions are proportional to γ , stemming entirely from the orbital-flavor nonconserving part of the kinetic energy.

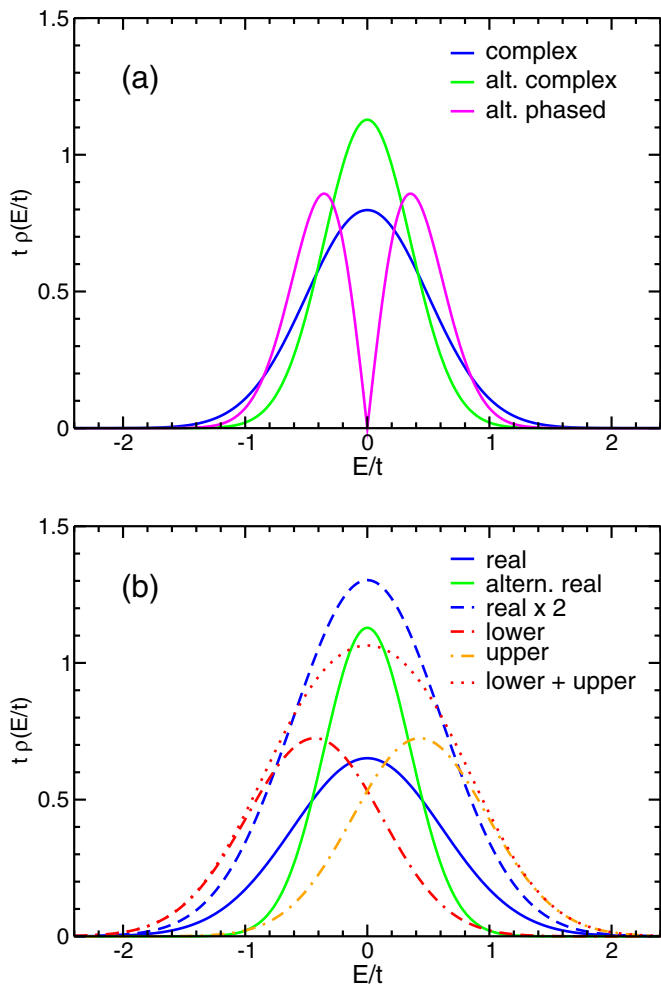


FIG. 2. DOSs of the various single-particle states: (a) for the complex-orbital single-particle states, $\rho_c(E)$, $\rho_{c,ao}(E)$, and $\rho_{c,ao}(E)$; (b) for the real-orbital single-particle states, $\rho_r(E)$, $\rho_{r,ao}(E)$, and $2\rho_r(E)$, and for the single-particle eigenstates, $\rho_\ell(E)$, $\rho_u(E)$, and $\rho_{\ell+u}(E)$.

The corresponding DOSs are again Gaussians, with widths $w_r = \sigma/2$ and $w_{r,ao} = \gamma/2\sqrt{2}$, respectively, where $\sigma = \sqrt{1 + \gamma^2/2}$. They are shown, for $\gamma = 1$, in Fig. 2(b) by the blue and green lines respectively. One may note that $w_{r,ao} = w_{c,ao}$, implying that the DOS of the alternating real-orbital single-particle states is identical to that of its complex-orbital counterpart shown in the upper panel.

C. Single-particle eigenstates

The creation operators for the single-particle *eigen*-states of the kinetic energy are seen from Eq. (2.20) to be simply proportional to the sum and difference of the phased single-particle operators,

$$\hat{d}_{\mathbf{k},\ell}^\dagger = \frac{1}{\sqrt{2}}(\hat{c}_{\mathbf{k}+}^\dagger + \hat{c}_{\mathbf{k}-}^\dagger), \quad (3.16)$$

$$\hat{d}_{\mathbf{k},u}^\dagger = \frac{-i}{\sqrt{2}}(\hat{c}_{\mathbf{k}+}^\dagger - \hat{c}_{\mathbf{k}-}^\dagger), \quad (3.17)$$

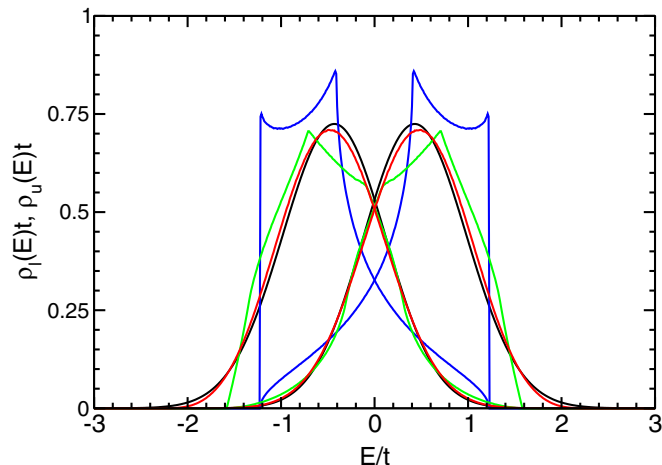


FIG. 3. Evolution of the DOS for the single-particle eigenstates ℓ and u of the e_g orbital model at $U = 0$ with increasing dimension: $d = 3$ (blue), $d = 5$ (green), $d = 11$ (red), and $d = \infty$ (black). The lines at finite d have been calculated by \mathbf{k} -space sampling, those at $d = \infty$ from Eq. (3.19).

and the corresponding energies of the lower (ℓ) and upper (u) subbands are

$$\varepsilon_{\ell,u}(\mathbf{k}) = -t(A_{\mathbf{k}} \pm \gamma B_{\mathbf{k}}), \quad (3.18)$$

where the $+$ ($-$) sign corresponds to the lower (upper) subband. We calculate the DOSs for the two subbands by evaluating the convolution of the DOSs corresponding to $A_{\mathbf{k}}$ and to the two branches of $B_{\mathbf{k}}$. Strictly this requires $A_{\mathbf{k}}$ and $B_{\mathbf{k}}$ to be uncorrelated [88], which is obviously not the case because both depend on \mathbf{k} , but we assume that this condition becomes irrelevant in the limit $d \rightarrow \infty$, and check the validity of this assumption afterwards (see below). We then obtain for the subband DOSs

$$\rho_{\ell,u}(E) = \frac{1}{\sqrt{2\pi}} \frac{2}{\sigma^2 t} e^{-\frac{1}{2}(\frac{2E}{t})^2} \times \left\{ 1 + \sqrt{\pi} \frac{\gamma E}{\sigma t} e^{(\frac{\gamma E}{\sigma t})^2} \left[\text{erf}\left(\frac{\gamma E}{\sigma t}\right) \mp 1 \right] \right\}, \quad (3.19)$$

where the upper (lower) sign corresponds to the ℓ (u) subband, and for their sum, which we will need later,

$$\rho_{\ell+u}(E) = \frac{2}{\sqrt{2\pi}} \frac{2}{\sigma^2 t} e^{-\frac{1}{2}(\frac{2E}{t})^2} \times \left\{ 1 + \sqrt{\pi} \frac{\gamma E}{\sigma t} e^{(\frac{\gamma E}{\sigma t})^2} \text{erf}\left(\frac{\gamma E}{\sigma t}\right) \right\}. \quad (3.20)$$

These DOSs are also shown, for $\gamma = 1$, in Fig. 2(b) by the dash-dotted red and orange lines and by the dotted red line, respectively.

We emphasize that the subbands $\{\varepsilon_\ell(\mathbf{k}), \varepsilon_u(\mathbf{k})\}$ are non-degenerate except for the \mathbf{k} points for which $B_{\mathbf{k}} = 0$. This feature found already at dimension $d = 3$ is generic and persists at increasing dimension up to $d = \infty$, contrary to the suggestion made in Ref. [89]. Figures 3 and 4 demonstrate this explicitly. In Fig. 3 the DOSs of the two subbands are seen to become smoother with increasing dimension but to remain

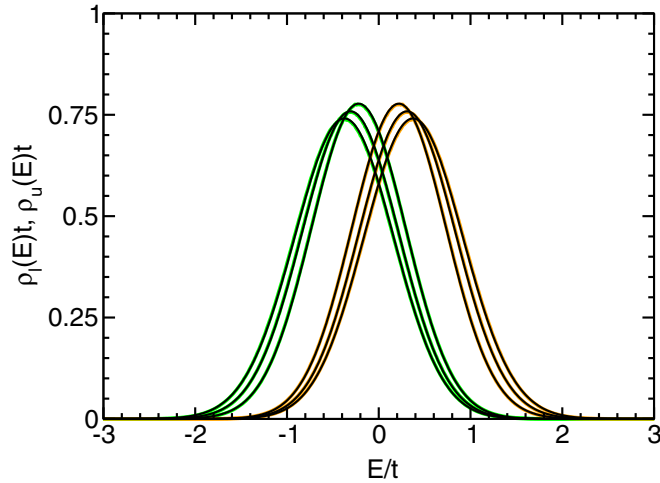


FIG. 4. Densities of states $\rho_{\ell,u}(E)$ for the single-particle eigenstates of the e_g orbital model at $U = 0$, for three values of the parameter γ ($\gamma = 0.25, 0.50$, and 0.75 , with increasing distance between the maxima), as given by the analytical expression (3.19) for $d \rightarrow \infty$ (thin black lines), and as calculated numerically at dimension $d = 21$, where green lines are used for $|\mathbf{k}, \ell\rangle$, orange lines are used for $|\mathbf{k}, u\rangle$.

distinct although they partly overlap. In Fig. 4 the evolution of the subband DOSs with γ is illustrated: in the spin Hubbard model, i.e., at $\gamma = 0$ (not shown), they necessarily coincide [compare Eq. (3.18)], while they are seen to get separated with their maxima moving away from each other with increasing γ and their maxima finally reaching a maximum distance of $\simeq 0.84$ at $\gamma = 1$ (not shown), i.e., in the full orbital model. This figure also demonstrates the validity of our assumption made in deriving Eq. (3.19): the colored lines, calculated by \mathbf{k} -space sampling of the dispersion Eq. (3.18) at 10^6 \mathbf{k} values, are indistinguishable from the black lines, calculated from the analytical $d = \infty$ expression (3.19).

We point out that the single-particle eigenstates given by Eqs. (3.16) and (3.17) are in fact *real* and could be considered as the “phased” real-orbital single-particle operators which are the counterpart to the phased complex-orbital single-particle operators defined by Eq. (2.19) above,

$$\hat{d}_{\mathbf{k},\ell}^\dagger = \cos(\phi_{\mathbf{k}}/2) \hat{c}_{\mathbf{k}\mathbf{x}_0}^\dagger + \sin(\phi_{\mathbf{k}}/2) \hat{c}_{\mathbf{k}\mathbf{y}_0}^\dagger, \quad (3.21)$$

$$\hat{d}_{\mathbf{k},u}^\dagger = -\sin(\phi_{\mathbf{k}}/2) \hat{c}_{\mathbf{k}\mathbf{x}_0}^\dagger + \cos(\phi_{\mathbf{k}}/2) \hat{c}_{\mathbf{k}\mathbf{y}_0}^\dagger, \quad (3.22)$$

as one readily verifies from Eqs. (2.19) and (2.1), or alternatively by recognizing that Eqs. (3.16) and (3.17) have the form of coherent orbital states like Eq. (2.4) with $\psi = 0$ and thus are given by Eq. (2.6). So they are represented in the “equatorial” plane [compare Fig. 1(c)] by an angle θ equal to the phase angle $\phi_{\mathbf{k}}$, which is entirely determined by the wave vector and therefore is in general not equal to any of the χ_n . An important consequence is that each of these single-particle states carries a finite orbital polarization, i.e., contributes at each lattice site to the value of the pseudospin in the xy plane

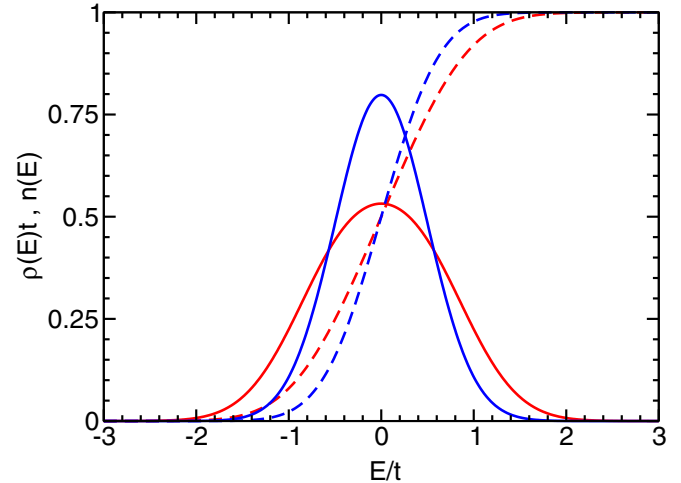


FIG. 5. Total DOS $\rho_{\ell+u}(E)$ (3.20) (solid lines) and the electron density per orbital/spin flavor $n(E)$ (dashed lines) in the unpolarized state, as obtained for the orbital e_g Hubbard model ($\gamma = 1$, red lines) and the spin Hubbard model ($\gamma = 0$, blue lines) at $d = \infty$.

[see Fig. 1(b)]:

$$\langle \mathbf{k}, \ell | \hat{T}_i^x | \mathbf{k}, \ell \rangle = -\langle \mathbf{k}, u | \hat{T}_i^x | \mathbf{k}, u \rangle = \frac{1}{2N} \cos \phi_{\mathbf{k}}, \quad (3.23)$$

$$\langle \mathbf{k}, \ell | \hat{T}_i^y | \mathbf{k}, \ell \rangle = -\langle \mathbf{k}, u | \hat{T}_i^y | \mathbf{k}, u \rangle = \frac{1}{2N} \sin \phi_{\mathbf{k}}, \quad (3.24)$$

$$\langle \mathbf{k}, \ell | \hat{T}_i^z | \mathbf{k}, \ell \rangle = \langle \mathbf{k}, u | \hat{T}_i^z | \mathbf{k}, u \rangle = 0. \quad (3.25)$$

It is noteworthy that while ℓ and u may properly be called (sub)bands, the polarization direction of the states in each band varies with \mathbf{k} , in contrast to the familiar feature of bands of particles carrying spin where the spin direction is the same for all states in a band.

D. Comparison with the spin Hubbard model

The expression (3.20) derived for the combined DOS of the two subbands $\rho_{\ell+u}(E)$ gives us the opportunity to compare the distribution of the single-particle eigenstates in the e_g orbital Hubbard with the one in the spin Hubbard model; see Fig. 5. In the orbital model the total DOS is broader and the total electron density $n(E)$ grows slower with increasing Fermi energy E . The plot already indicates that the kinetic energy in the orbital model at a particular density n , obtained by filling the two subbands up to the same Fermi energy, is lower than the kinetic energy obtained at the same density in the spin model. This difference is a manifestation of the flavor nonconserving hopping which opens an extra channel for the kinetic energy and thus enhances it in the orbital model.

E. Kinetic energies

Before taking electron correlations into account, we examine the kinetic energy of the various trial states $|\Phi_0\rangle$ built from the single-particle states discussed above, and identify the most favorable states in the absence of Coulomb interactions. We consider on the one hand uniformly polarized ordered states, obtained by filling a single band (or, in the cases of alternating order, subsequently the lower and upper

band corresponding to the same sublattice occupation), and on the other hand unpolarized “paraorbital” states, obtained by filling two degenerate bands up to the same Fermi energy; compare Eq. (3.3). For each such trial state the particle density n and the kinetic energy E_{kin} as a function of the Fermi energy E_F are given by

$$n(E_F) = \int_{-\infty}^{E_F} \rho(E) dE, \quad (3.26)$$

$$E_{\text{kin}}(E_F) = \int_{-\infty}^{E_F} E \rho(E) dE, \quad (3.27)$$

where $\rho(E)$ is the DOS of the corresponding band(s) of single-particle states. Only the density range $0 \leq n \leq 1$ will be considered since n and $2 - n$ are equivalent because of particle-hole symmetry.

We begin with the *ordered* orbital phases built from *complex-orbital* single-particle states. The simplest one is the complex ferro-orbital state $|\Phi_0^{\text{FOc}}\rangle$ obtained by filling the $|\mathbf{k}+\rangle$ band (or the $|\mathbf{k}-\rangle$ band). The complex alternating-orbital state $|\Phi_0^{\text{AOc}}\rangle$ is [compare Eqs. (3.7) and (3.8)] obtained by filling consecutively the $|\mathbf{k}, +-, \ell\rangle$ band and the $|\mathbf{k}', +-, u\rangle$ band, and the phased complex alternating-orbital state $|\Phi_0^{\text{AO}\check{c}}\rangle$ is built similarly from the $\hat{c}_{\mathbf{k}+-, \ell}^\dagger$ and $\hat{c}_{\mathbf{k}'+-, u}^\dagger$ single-particle states.

Moving on to the *unpolarized* states we have the complex paraorbital state POC, obtained by filling simultaneously the $|\mathbf{k}+\rangle$ band and the $|\mathbf{k}-\rangle$ band, the complex alternating paraorbital state PAOC, obtained by filling simultaneously the $|\mathbf{k}, +-, \ell\rangle$ band and the $|\mathbf{k}', -+, \ell\rangle$ band [compare Eq. (3.7)], i.e., from the lower band only, and finally the similarly defined phased complex alternating paraorbital state PAO \check{c} . Figure 6(a) shows the kinetic energies of these six states plotted versus the particle density.

Next we consider the trial states built from *real-orbital* single-particle states, again beginning with the *ordered* phases. Analogous to the complex trial states above we have the real ferro-orbital state $|\Phi_0^{\text{FOr}}\rangle$ obtained by filling the $|\mathbf{k}x_0\rangle$ band (or alternatively the $|\mathbf{k}\bar{x}_0\rangle$ band) and the real alternating-orbital state $|\Phi_0^{\text{AOr}}\rangle$ obtained by filling consecutively the $|\mathbf{k}, x_0\bar{x}_0, \ell\rangle$ band and the $|\mathbf{k}', x_0\bar{x}_0, u\rangle$ band; compare Eqs. (3.7) and (3.8). Here the *unpolarized* states are the real paraorbital state POr, with equally filled $|\mathbf{k}x_0\rangle$ band and $|\mathbf{k}\bar{x}_0\rangle$ band, and the real alternating paraorbital state PAOr, with the $|\mathbf{k}, x_0\bar{x}_0, \ell\rangle$ band and the $|\mathbf{k}', \bar{x}_0x_0, \ell\rangle$ band filled equally. The kinetic energies of these four states plotted versus particle density are shown in Fig. 6(b).

The n dependence of the various kinetic energies can be understood as follows. For all ordered states for which the single-particle DOS is Gaussian, which includes the FOc, AOc, FOr, and AOr states, the particle density and kinetic energy take the form

$$n(E_F) = \frac{1}{2} \left[1 + \text{erf} \left(\frac{E_F}{wt\sqrt{2}} \right) \right], \quad (3.28)$$

$$E_{\text{kin}}(E_F) = -\frac{wt}{\sqrt{2\pi}} \exp \left[-\frac{1}{2} \left(\frac{E_F}{wt} \right)^2 \right], \quad (3.29)$$

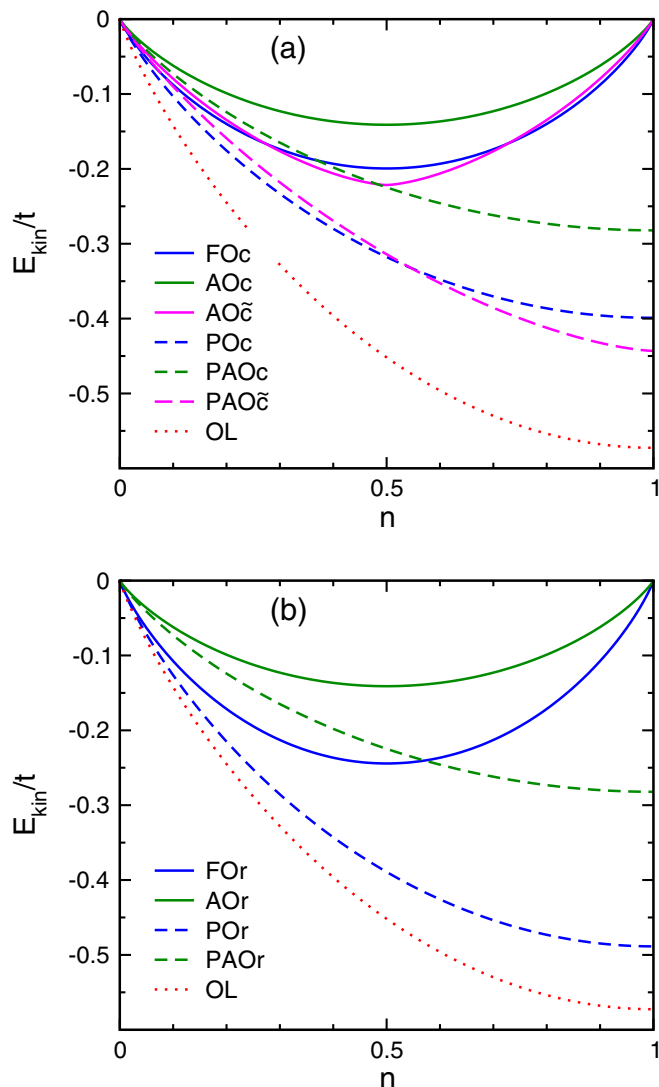


FIG. 6. Kinetic energies E_{kin} in the limit $d \rightarrow \infty$ of the orbital ordered and the paraorbital states of the e_g Hubbard model (2.9) (i.e., $\gamma = 1$) at $U = 0$ for increasing electron density n , compared with that of the orbital liquid state. (a) Phases with *complex* orbitals: ferro-orbital FOc (solid blue line), alternating-orbital AOc (solid green line), phased alternating-orbital AO \check{c} (solid cyan line), paraorbital POc (dashed blue line), alternating paraorbital PAOc (dashed green line), phased alternating paraorbital PAO \check{c} (dashed cyan line), and orbital liquid OL (dotted red line). (b) Phases with *real* orbitals: ferro-orbital FOr (solid blue line), alternating-orbital AOr (solid green line), paraorbital POr (dashed blue line), alternating paraorbital PAOr (dashed green line), and orbital liquid OL [dotted red line, the same as in (a)].

where erf is the error function. Formally, inversion of Eq. (3.28) gives

$$E_F(n) = wt\sqrt{2} \text{inverf}(2n - 1), \quad (3.30)$$

where inverf is the inverse error function, and, inserting this into Eq. (3.29), one obtains

$$E_{\text{kin}}(n) = -\frac{wt}{\sqrt{2\pi}} \exp(-[\text{inverf}(2n - 1)]^2). \quad (3.31)$$

This demonstrates that the shape of $E_{\text{kin}}(n)$ is the same for the states mentioned above, as is evident in Fig. 6, and that the only difference is in the width prefactor w , which also determines the value of the minimum, $-wt/\sqrt{2\pi}$, at $n = 1/2$. The only exception is the AO \check{c} state for which the Rayleigh distribution type DOS Eq. (3.12) leads to

$$n^{\text{AO}\check{c}}(E_F) = \frac{1}{2} \left[1 + \text{sgn}(E_F) \left(1 - e^{-\left(\frac{2E_F}{\gamma t}\right)^2} \right) \right], \quad (3.32)$$

$$E_{\text{kin}}^{\text{AO}\check{c}}(E_F) = -\frac{t}{\sqrt{2\pi}} \frac{\gamma\pi}{4\sqrt{2}} \left[1 - \text{erf}\left(\frac{2|E_F|}{\gamma t}\right) + \frac{2}{\sqrt{\pi}} \frac{2|E_F|}{\gamma t} e^{-\left(\frac{2E_F}{\gamma t}\right)^2} \right]. \quad (3.33)$$

As Fig. 6(a) shows, this makes the AO \check{c} state have lower kinetic energy than the FO \check{c} state close to quarter-filling, i.e., in the interval $0.25 < n < 0.75$. This can be understood from the fact that the DOS of the phased complex-orbital single-particle states has more weight at more negative energies; see Fig. 2(a). However, as seen in Fig. 6(b), it is the FO \check{r} state that clearly has the lowest kinetic energy of all ordered states due to its large width, with minimum energy $-0.2443t$, whereas the minimum for the AO \check{c} state is only $-0.2216t$; see Eq. (3.33). The basic reason for the difference is that the FO \check{r} state benefits fully from the orbital-flavor conserving hopping channel and also partially from the nonconserving channel [compare Eq. (3.13)], while the AO \check{c} state benefits fully from the orbital-flavor nonconserving channel but not at all from the conserving channel; cf. Eq. (3.10).

As regards the unpolarized states one may observe that for every paraorbital state PX its kinetic energy is related to that of the associated ordered state X by

$$E_{\text{kin}}^{\text{PX}}(n) = 2E_{\text{kin}}^{\text{X}}(n/2), \quad (3.34)$$

which follows directly from the defining equations (3.26) and (3.27). Equation (3.34) implies that the relative magnitude of the kinetic energies of the unpolarized states is the same as that of the ordered states, as indeed seen in Fig. 6. In particular, the PO \check{r} state has the lowest kinetic energy of all paraorbital disordered phases, for the same reason as the FO \check{r} state is the lowest-energy ordered state. Also, the paraorbital states have considerably lower kinetic energy than their ordered counterparts, but they will get renormalized at finite U whereas the ordered states will not.

Finally we consider the trial state built from the single-particle *eigenstates* by filling the lower and the upper subbands up to the same Fermi energy, written down here

explicitly [compare Eqs. (3.16)–(3.18)]:

$$|\Phi_0^{\text{OL}}\rangle = \prod_{\mathbf{k}; \varepsilon_\ell(\mathbf{k}) < E_F} \prod_{\mathbf{k}'; \varepsilon_u(\mathbf{k}') < E_F} \hat{d}_{\mathbf{k},\ell}^\dagger \hat{d}_{\mathbf{k}',u}^\dagger |0\rangle. \quad (3.35)$$

This state we call the OL state because it is unpolarized in the following remarkable way.

Whereas all single-particle states in $|\Phi_0^{\text{OL}}\rangle$ are polarized individually [compare Eqs. (3.23) and (3.24)], the variation with \mathbf{k} makes their contributions to the pseudospin add up to zero at each lattice site, at any filling $n(E_F)$, and for each subband ℓ and u separately. This follows from the following considerations (for a more detailed proof, see the Appendix):

(i) For every single-particle state $|\mathbf{k}, \ell\rangle$ from the lowest subband which is occupied in $|\Phi_0^{\text{OL}}\rangle$ because it satisfies $\varepsilon_\ell(\mathbf{k}) < E_F$, all single-particle states $|\mathbf{k}'_n, \ell\rangle$ with wave vectors \mathbf{k}'_n generated from \mathbf{k} by successive cyclic permutations of its components are also occupied. This holds because both $A_{\mathbf{k}}$ and $B_{\mathbf{k}}$ are invariant under such permutations [compare Eqs. (2.14) and (2.16)], implying that $\varepsilon_\ell(\mathbf{k}'_n) = \varepsilon_\ell(\mathbf{k})$, and it follows that $\varepsilon_\ell(\mathbf{k}'_n) < E_F$. The same reasoning applies for the upper subband u ;

(ii) Under each such transformation $\mathbf{k} \mapsto \mathbf{k}'_n$ the corresponding phase angle is transformed as $\phi_{\mathbf{k}} \mapsto \phi_{\mathbf{k}} + 4n\pi/d$, so summing $\exp(i\phi_{\mathbf{k}'_n})$ over all \mathbf{k}'_n yields 0, and the compensation of the contributions to the pseudospin follows; compare again Eqs. (3.23) and (3.24).

Therefore, even though the densities in the two partially filled subbands are different, $n_\ell(E_F) > n_u(E_F)$, as recognized from the DOSs shown in Fig. 2(b), the OL state is unpolarized, because each subband is unpolarized by itself at any filling. This mechanism is entirely different from the compensation of two oppositely polarized bands at equal filling as occurs for paraorbital (or paramagnetic) states.

We emphasize that the reasoning above is not specific for $d = \infty$ but holds in any dimension, and so the resulting absence of polarization in both bands is a characteristic feature of the OL *per se*. It is associated with the fact that the OL transforms as A_1 under the symmetry group C_d [is invariant under $U(1)$ in the limit $d \rightarrow \infty$] and implies that *the OL phase protects the (hyper)cubic symmetry*. We further point out that there is necessarily double occupancy in $|\Phi_0^{\text{OL}}\rangle$. This is obvious from the fact that the single-particle states in $|\Phi_0^{\text{OL}}\rangle$ do not correspond to a single common direction in the “equatorial” plane of Fig. 1(c) because of the variation of $\phi_{\mathbf{k}}$ with the wave vector \mathbf{k} .

The relevant DOS from which to obtain the particle density and the kinetic energy in the OL state is $\rho_{\ell+u}(E)$, Eq. (3.20). One finds

$$n_{\text{OL}}(E_F) = 1 + \text{erf}\left(\frac{\sqrt{2}E_F}{t}\right) - \frac{\gamma}{\sigma\sqrt{2}} e^{-2\left(\frac{E_F}{\sigma t}\right)^2} \text{erf}\left(\frac{\gamma E_F}{\sigma t}\right), \quad (3.36)$$

$$E_{\text{kin:OL}}(E_F) = -\frac{t}{\sqrt{2\pi}} \left\{ e^{-2\left(\frac{E_F}{t}\right)^2} + \gamma\sqrt{\pi} \left[\frac{E_F}{\sigma t} e^{-2\left(\frac{E_F}{\sigma t}\right)^2} \text{erf}\left(\frac{\gamma E_F}{\sigma t}\right) + F\left(\gamma; \frac{|E_F|}{\sigma t}\right) \right] \right\}, \quad (3.37)$$

where

$$F(\gamma; x) = \int_x^\infty e^{-2y^2} \text{erf}(\gamma y) dy. \quad (3.38)$$

The function $F(\gamma; x)$ has to be calculated numerically. Since $F(1; 0) = \frac{1}{\sqrt{2\pi}} [\frac{\pi}{2} - \tan^{-1}(\sqrt{2})] = 0.245541$ [90], we have rewritten Eq. (3.38) at $\gamma = 1$ as

$$F(1; x) = 0.245541 - \int_0^x e^{-2y^2} \operatorname{erf}(y) dy. \quad (3.39)$$

to perform the calculation for the full orbital case.

The kinetic energy of the OL state is included in both Figs. 6(a) and 6(b), and is seen to be lower than that of any other trial state, remarkably including the lowest-energy complex paraorbital and real paraorbital states. The explanation is similar to that above for the FOr and the POr states. The OL state fully captures all kinetic energy available in the orbital Hubbard model (2.9), both from the orbital-flavor conserving hopping channel and from the nonconserving hopping channel; cf. Eq. (3.18). This is a strong hint that the OL phase could be favored also in the presence of electron interactions. To establish the phase with the lowest overall energy we need to consider the energy renormalization of the paraorbital states and the OL state in the presence of the Coulomb interaction, i.e., at finite U .

IV. CORRELATIONS BY THE GUTZWILLER METHOD

The original analysis of the Gutzwiller approach in the limit $d \rightarrow \infty$, including the proof that the Gutzwiller approximation becomes exact in that limit, was carried out specifically for the spin Hubbard model, implying the implicit assumption of $SU(2)$ symmetry [3,8,9]. We therefore need to investigate which modifications are required in the orbital case where we have only C_d symmetry, and check if the proof of exactness still holds.

A. General derivation at dimension d

Electron correlations due to the on-site Hubbard repulsion U will be implemented using the wave function introduced by Gutzwiller,

$$|\Psi(g)\rangle = g^{\hat{D}} |\Phi_0\rangle = \prod_i (1 - (1-g)\hat{D}_i) |\Phi_0\rangle, \quad (4.1)$$

with

$$\hat{D} = \sum_i \hat{D}_i, \quad \hat{D}_i = \hat{n}_{i+} \hat{n}_{i-}, \quad (4.2)$$

where the variational parameter g is determined by minimizing the energy [6–9],

$$E(g) = \frac{\langle \Psi(g) | \mathcal{H}_d | \Psi(g) \rangle}{\langle \Psi(g) | \Psi(g) \rangle}. \quad (4.3)$$

First, we consider here the general case and derive the propagator and self-energy. In the present case the fermion (orbital) flavor is not conserved and we introduce a propagator,

$$\mathcal{P}_{ij;\alpha\beta} = \frac{\langle \Psi | \hat{c}_{i\alpha}^\dagger \hat{c}_{j\beta} | \Psi \rangle}{\langle \Psi(g) | \Psi(g) \rangle}, \quad (4.4)$$

which we allow to have, at least in principle, *nonzero off-diagonal matrix elements with respect to flavor* (i.e., $\alpha \neq \beta$). Following Metzner [9], one finds the following expression for

the matrix elements:

$$\mathcal{P}_{ij;\alpha\beta} = \{c_{i\alpha}^\dagger c_{j\beta} [1 - (1-g)(n_{i\bar{\alpha}} + n_{j\bar{\beta}}) + (1-g)^2(n_{i\bar{\alpha}}n_{j\bar{\beta}} + \delta_{ij}\delta_{\alpha\beta}n_{i\bar{\alpha}})]X\}_0^c, \quad (4.5)$$

where

$$X \equiv 1 + \sum_{m=1}^{\infty} \frac{(g^2 - 1)^m}{m!} \sum_{g_1, \dots, g_m} D_{g_1}, \dots, D_{g_m}. \quad (4.6)$$

Similarly, the bare propagator is defined by

$$\mathcal{P}_{ij;\alpha\beta}^0 = \langle \Phi_0 | \hat{c}_{i\alpha}^\dagger \hat{c}_{j\beta} | \Phi_0 \rangle = \{c_{i\alpha}^\dagger c_{j\beta}\}_0^c. \quad (4.7)$$

Here \mathcal{P}^0 is, like \mathcal{P} , an $N \times N \times 2 \times 2$ matrix with off-diagonal elements with respect to orbital flavor generated by the off-diagonal hopping in orbital space. We emphasize that the curly brackets $\{\dots\}_0^c$ in Eqs. (4.5) and (4.7) denote the sum over all connected products of anticommuting contractions, evaluated in the trial state $|\Phi_0\rangle$, and thus the $c_{i\alpha}, \dots$ symbols are Grassman variables and not the fermion operators $\hat{c}_{i\alpha}, \dots$.

Next we define the self-energy \mathcal{S} . Here \mathcal{S}_{ij} is a 2×2 matrix with off-diagonal elements in orbital space. The elements of the self-energy \mathcal{S} are therefore different from those for the RVB wave function [9], and include the specific last term in the defining equation

$$\mathcal{S}_{ij;\alpha\beta} = \{[(1-g)^2 c_{i\alpha}^\dagger n_{i\bar{\alpha}} c_{j\beta} n_{j\bar{\beta}} - \delta_{ij}(g^2 - 1)(\delta_{\alpha\beta} n_{i\bar{\alpha}} - \delta_{\alpha\bar{\beta}} c_{i\alpha}^\dagger c_{j\beta})]X\}_0^c. \quad (4.8)$$

The self-energy gives the double occupancy

$$\bar{d}_i = \frac{1}{2} \frac{g^2}{1-g^2} \operatorname{Tr}_\alpha (\mathcal{S} \mathcal{P}^0)_{ii}. \quad (4.9)$$

The further derivation, following closely the case of the RVB state considered by Metzner [9], leads after some algebraic manipulations to the propagator in real space between sites i and j ,

$$\mathcal{P}_{ij} = \mathcal{P}_{ij}^0 + \delta_{ij} \left[\frac{1-g}{1+g} (\mathcal{S} \mathcal{P}^0)_{ii} \delta_{\alpha\beta} - \frac{\mathcal{S}_{ii}}{(1+g)^2} \right] + \left[\left(\mathcal{P}^0 - \frac{1}{1+g} \right) \mathcal{S} \left(\mathcal{P}^0 - \frac{1}{1+g} \right) \right]_{ij}. \quad (4.10)$$

Here in the first local term at site i only the diagonal elements of the matrix $\mathcal{S} \mathcal{P}^0$ contribute, as indicated by $\delta_{\alpha\beta}$.

The first term in Eq. (4.5) is related to the self-energy \mathcal{S} by

$$\{c_{i\alpha}^\dagger c_{j\beta} X\}_0^c \equiv (\mathcal{P}^0 + \mathcal{P}^0 \mathcal{S} \mathcal{P}^0)_{ij;\alpha\beta}. \quad (4.11)$$

Finally, we define a ‘‘proper self-energy’’ \mathcal{S}^* as the sum over all one-particle irreducible diagrams contributing to \mathcal{S} ; the two self-energies are then related by a Dyson equation,

$$\mathcal{S} = \mathcal{S}^* + \mathcal{S}^* \circ \mathcal{P}^0 \circ \mathcal{S}. \quad (4.12)$$

After introducing a renormalized propagator

$$\bar{\mathcal{P}} = \mathcal{P}^0 + \mathcal{P}^0 \circ \mathcal{S} \circ \mathcal{P}^0, \quad (4.13)$$

one finds that, owing to Eq. (4.12), it satisfies

$$\bar{\mathcal{P}} = \mathcal{P}^0 + \mathcal{P}^0 \circ \mathcal{S}^* \circ \bar{\mathcal{P}}. \quad (4.14)$$

The site-diagonal matrix elements of \mathcal{S} are related to those of $\overline{\mathcal{P}}$ as follows:

$$\mathcal{S}_{ii;\alpha\alpha} = (1 - g^2)\overline{\mathcal{P}}_{ii;\bar{\alpha}\bar{\alpha}}, \quad (4.15)$$

$$\mathcal{S}_{ii;\alpha\bar{\alpha}} = -(1 - g^2)\overline{\mathcal{P}}_{ii;\alpha\bar{\alpha}}. \quad (4.16)$$

B. Single-site collapse at $d = \infty$

Similarly to the spin Hubbard model at $d \rightarrow \infty$, the diagrams describing the perturbation expansion of \mathcal{S}^* with respect to the local interaction U collapse. Then the lattice sums reduce to summations of terms in which all indices coincide on the same lattice site, and the proper self-energy becomes site diagonal, i.e., $\mathcal{S}_{ij}^* = \delta_{ij}\mathcal{S}_{ii}^*$. The collapse permits the matrix elements of \mathcal{S}_{ii}^* (with respect to the orbital label) to be expressed in terms of those of the on-site matrix elements of $\overline{\mathcal{P}}_{ii}$ defined above. One finds, in matrix form,

$$\mathcal{S}_{ii}^* = f \begin{pmatrix} -\overline{\mathcal{P}}_{ii;--} & +\overline{\mathcal{P}}_{ii;+-} \\ +\overline{\mathcal{P}}_{ii;-+} & -\overline{\mathcal{P}}_{ii;++} \end{pmatrix}. \quad (4.17)$$

We emphasize that \mathcal{S}_{ii}^* is not yet necessarily independent of i . Here the factor f is

$$f = \frac{1 - [1 + 4(1 - g^2)\det \overline{\mathcal{P}}_{ii}]^{1/2}}{2 \det\{\overline{\mathcal{P}}_{ii}\}}, \quad (4.18)$$

$$\begin{aligned} \mathcal{P}(\mathbf{k}) &= \mathcal{P}^0(\mathbf{k}) + \sum_{\mathbf{k}'} \left[\frac{1-g}{1+g} (\mathcal{S}(\mathbf{k}')\mathcal{P}^0(\mathbf{k}'))_{\alpha\alpha} \delta_{\alpha\beta} - \frac{\mathcal{S}(\mathbf{k}')}{(1+g)^2} \right] \\ &+ \left[\left(\mathcal{P}^0(\mathbf{k}) - \frac{1}{1+g} \right) \mathcal{S}(\mathbf{k}) \left(\mathcal{P}^0(\mathbf{k}) - \frac{1}{1+g} \right) \right]. \end{aligned} \quad (4.20)$$

Consider now a homogeneous state where $\mathcal{S}_{ii}^* \equiv \mathcal{S}^*$ is site independent, and we may use a shorthand notation for its matrix elements,

$$\mathcal{S}^* = \begin{pmatrix} \mathcal{S}_+^* & R^* \\ (R^*)^+ & \mathcal{S}_-^* \end{pmatrix} = \begin{pmatrix} \mathcal{S}_+^* & |R^*|e^{i\phi} \\ |R^*|e^{-i\phi} & \mathcal{S}_-^* \end{pmatrix}. \quad (4.21)$$

Using the Dyson equation for $\overline{\mathcal{P}}$ in Eq. (4.14), $\overline{\mathcal{P}}(\mathbf{k})$ can be expressed (in \mathbf{k} -space) explicitly in terms of $\mathcal{P}^0(\mathbf{k})$ and $\mathcal{S}^*(\mathbf{k})$,

$$\overline{\mathcal{P}}(\mathbf{k}) = \frac{1}{N_{\mathbf{k}}} \left[\mathcal{P}^0(\mathbf{k}) - \det \mathcal{P}^0(\mathbf{k}) \begin{pmatrix} \mathcal{S}_-^* & -R^* \\ -(R^*)^+ & \mathcal{S}_+^* \end{pmatrix} \right], \quad (4.22)$$

where the normalizing prefactor $N_{\mathbf{k}}$ is

$$N_{\mathbf{k}} = 1 - \text{Tr}_{\alpha} \{ \mathcal{S}^* \mathcal{P}^0(\mathbf{k}) \} + (\det \mathcal{S}^*) \det \mathcal{P}^0(\mathbf{k}). \quad (4.23)$$

It depends on the occupancy of the single-particle states at wave vector \mathbf{k} in the many-particle trial state $|\Phi\rangle$. Upon solving for \mathcal{S}_+^* , \mathcal{S}_-^* , R^* , and $(R^*)^+$, one obtains the self-energy from

$$\mathcal{S}(\mathbf{k}) = \frac{1}{N_{\mathbf{k}}} \left[\mathcal{S}^* - \det \mathcal{S}^* \begin{pmatrix} \mathcal{P}^0(\mathbf{k})_{--} & -\mathcal{P}^0(\mathbf{k})_{+-} \\ -\mathcal{P}^0(\mathbf{k})_{-+} & \mathcal{P}^0(\mathbf{k})_{++} \end{pmatrix} \right], \quad (4.24)$$

upon which it is straightforward to write down explicitly the expression for the propagator $\mathcal{P}(\mathbf{k})$ and calculate all quantities of physical interest.

and upon inversion

$$\overline{\mathcal{P}}_{ii} = \frac{1}{(1 - g^2) - \det \mathcal{S}_{ii}^*} \begin{pmatrix} +\mathcal{S}_{ii;--}^* & -\mathcal{S}_{ii;+-}^* \\ -\mathcal{S}_{ii;-+}^* & +\mathcal{S}_{ii;++}^* \end{pmatrix}. \quad (4.19)$$

Equating this to the site-diagonal part of $\overline{\mathcal{P}}$ as obtained from Eq. (4.14) generates two equations which together determine \mathcal{S}^* , for any given \mathcal{P}^0 and g . Next, Eq. (4.12) gives the self-energy \mathcal{S} , which finally determines the propagator via Eq. (4.10) and the double-occupancy using Eq. (4.9), and thus the total energy at any given electron filling n .

C. Momentum space representation

As we shall be mainly interested in translation invariant states, it is expedient to Fourier transform all variables of interest upon which matrix products with respect to site indices turn into ordinary products in \mathbf{k} -space, e.g., Eq. (4.10) becomes

V. GUTZWILLER RENORMALIZATION

A. Ordered states

As an example, we consider an ordered, i.e., polarized, state with complex orbitals, Oc,

$$|\Phi_0^{\text{Oc}}\rangle = \prod_{\mathbf{k} \in \mathcal{K}_+} \hat{c}_{\mathbf{k}+}^{\dagger} \prod_{\mathbf{q} \in \mathcal{K}_-} \hat{c}_{\mathbf{q}-}^{\dagger} |0\rangle. \quad (5.1)$$

It contains fixed numbers of electrons n_+^0 and n_-^0 in $|i+\rangle$ and $|i-\rangle$ states ($n_+^0 \geq n_-^0$), respectively,

$$n_+^0 = \sum_{\mathbf{k} \in \mathcal{K}_+} n_{\mathbf{k},+}^0, \quad n_-^0 = \sum_{\mathbf{q} \in \mathcal{K}_-} n_{\mathbf{q},-}^0, \quad (5.2)$$

which determine the total electron number n_0 and orbital polarization m_0 ,

$$n_0 = n_+^0 + n_-^0, \quad m_0 = n_+^0 - n_-^0. \quad (5.3)$$

The state (5.1) includes both full polarization, $n_-^0 = 0$ and $n_0 = m_0 = n_+^0$, i.e., the complex ferro-orbital state FOC, and zero polarization, $n_{0\pm} = \frac{1}{2}n_0$, $m_0 = 0$, i.e., the complex paraorbital state POC.

The bare propagator is a diagonal 2×2 matrix in the orbital $\{|+\rangle, |-\rangle\}$ basis, i.e., $\mathcal{P}_{\alpha\beta}^0(\mathbf{k}) = \delta_{\alpha\beta} n_{\mathbf{k}\alpha}^0$, and thus $\det\{\mathcal{P}^0(\mathbf{k})\} = n_{\mathbf{k}+}^0 n_{\mathbf{k}-}^0$. Consequently, the explicit form of the

matrix elements of $\bar{\mathcal{P}}(\mathbf{k})$ and $\bar{\mathcal{P}}_{ii} \equiv \bar{P}$ simplify, and the equations following from Eqs. (4.22) and (4.19) reduce to

$$\begin{aligned} \bar{P}_{++} &= \frac{1}{N} \sum_{\mathbf{k}} \bar{\mathcal{P}}(\mathbf{k})_{++} \\ &= \frac{1}{N} \sum_{\mathbf{k}} \left[\frac{n_{\mathbf{k}+}^0 (1 - n_{\mathbf{k}-}^0)}{1 - S_+^*} + \frac{n_{\mathbf{k}+}^0 n_{\mathbf{k}-}^0 (1 - S_-^*)}{(1 - S_+^*)(1 - S_-^*) - |R^*|^2} \right] \\ &= \frac{S_-^*}{1 - g^2 - (S_+^* S_-^* - |R^*|^2)}, \end{aligned} \quad (5.4)$$

$$\begin{aligned} \bar{P}_{+-} &= \frac{1}{N} \sum_{\mathbf{k}} \bar{\mathcal{P}}(\mathbf{k})_{+-} \\ &= \frac{1}{N} \sum_{\mathbf{k}} \frac{n_{\mathbf{k}+}^0 n_{\mathbf{k}-}^0 R^*}{(1 - S_+^*)(1 - S_-^*) - |R^*|^2} \\ &= -\frac{R^*}{1 - g^2 - (S_+^* S_-^* - |R^*|^2)}, \end{aligned} \quad (5.5)$$

$$\begin{aligned} \bar{P}_{--} &= \frac{1}{N} \sum_{\mathbf{k}} \bar{\mathcal{P}}(\mathbf{k})_{--} \\ &= \frac{1}{N} \sum_{\mathbf{k}} \left[\frac{n_{\mathbf{k}-}^0 (1 - n_{\mathbf{k}+}^0)}{1 - S_-^*} + \frac{n_{\mathbf{k}+}^0 n_{\mathbf{k}-}^0 (1 - S_+^*)}{(1 - S_+^*)(1 - S_-^*) - |R^*|^2} \right] \\ &= \frac{S_+^*}{1 - g^2 - (S_+^* S_-^* - |R^*|^2)}, \end{aligned} \quad (5.6)$$

From Eq. (5.5) it follows that $R^* = 0$, and Eqs. (5.4) and (5.6) are simplified to

$$\frac{n_+^{0s}}{1 - S_+^*} + \frac{d^0}{1 - S_+^*} = \frac{S_-^*}{1 - g^2 - S_+^* S_-^*}, \quad (5.7)$$

$$\frac{n_-^{0s}}{1 - S_-^*} + \frac{d^0}{1 - S_-^*} = \frac{S_+^*}{1 - g^2 - S_+^* S_-^*}, \quad (5.8)$$

where n_α^{0s} is the number of singly occupied \mathbf{k} points of flavor $\alpha \in \{+, -\}$ and d^0 is the number of doubly occupied \mathbf{k} points, hence

$$n_\alpha^0 = n_\alpha^{0s} + d^0. \quad (5.9)$$

After some algebraic manipulation one finds

$$n_+^0 \frac{S_+^*}{1 - S_+^*} = n_-^0 \frac{S_-^*}{1 - S_-^*}, \quad (5.10)$$

and the solution for S_+^* and S_-^* can be found.

Using the simplified (because of $R^* = 0$) expressions for $S(\mathbf{k})$ and $\bar{\mathcal{P}}(\mathbf{k})$ one finds

$$\mathcal{P}(\mathbf{k})_{\alpha\beta} = \delta_{\alpha\beta} n_{\mathbf{k}\alpha} = \delta_{\alpha\beta} [q_\alpha(g) n_{\mathbf{k}\alpha}^0 + b_\alpha], \quad (5.11)$$

with

$$q_\alpha(g) \equiv 1 - \frac{S_\alpha^*}{1 + g^2} \left(1 - \frac{g^2}{1 - S_\alpha^*} \right), \quad (5.12)$$

$$b_\alpha \equiv [1 - q_\alpha(g)] n_\alpha^0. \quad (5.13)$$

This is the Gutzwiller approximation for the ordered state Eq. (5.1). Note that

$$n_\alpha = \frac{1}{N} \sum_{\mathbf{k}} n_{\mathbf{k}\alpha} = q_\alpha n_\alpha^0 + b_\alpha = n_\alpha^0, \quad (5.14)$$

i.e., the Luttinger theorem is satisfied. The average double occupancy is given by

$$\bar{d} = \frac{g^2}{1 - g^2} \frac{S_+^*}{1 - S_+^*} n_{0+} = \frac{g^2}{1 - g^2} \frac{S_-^*}{1 - S_-^*} n_{0-}. \quad (5.15)$$

One recognizes that the above results are identical to those obtained in the spin case, i.e., for SU(2) symmetry.

For any other trial state built from a single pair of orthogonal orbitals [cf. Eq. (2.4)],

$$|\Phi_0^{\psi\theta}\rangle = \prod_{\mathbf{k} \in \mathcal{K}} \hat{c}_{\mathbf{k}}^\dagger(\psi, \theta) \prod_{\mathbf{q} \in \mathcal{Q}} \hat{c}_{\mathbf{k}}^\dagger(\psi + \pi, \theta + \pi) |0\rangle, \quad (5.16)$$

one obtains exactly analogous results when similarly writing all expressions in terms of the corresponding orbital basis. So, e.g., for the real Or states built from $\{|\mathbf{k}x_0\rangle\}$ and $\{|\mathbf{q}\bar{x}_0\rangle\}$ single-particle states [compare Eq. (5.1)], one has

$$n_{\mathbf{k}x_0} = q_{x_0}(g) n_{\mathbf{k}x_0}^0 + b_{x_0}; \quad (5.17)$$

compare Eq. (5.11). The renormalization $q_{x_0}(g)$ and the background constant density b_{x_0} are straightforwardly obtained from $q_\alpha(g)$ and b_α by the corresponding orbital transformation.

B. Orbital liquid state

Next we consider the OL state introduced above [see Eq. (3.35)],

$$|\Phi_0^{\text{OL}}\rangle = \prod_{\mathbf{k}; \varepsilon_\ell(\mathbf{k}) < E_F} \prod_{\mathbf{k}'; \varepsilon_u(\mathbf{k}') < E_F} \hat{d}_{\mathbf{k},\ell}^\dagger \hat{d}_{\mathbf{k}',u}^\dagger |0\rangle, \quad (5.18)$$

where \mathbf{k} and \mathbf{k}' label the occupied states from the lower (ℓ) and upper (u) subband, and both subbands are occupied up to the same Fermi energy E_F .

The free propagator is, in the $(+, -)$ basis,

$$\mathcal{P}_{\mathbf{k}}^0 = \frac{1}{2} \begin{pmatrix} n_{\mathbf{k},\ell}^0 + n_{\mathbf{k},u}^0 & (n_{\mathbf{k},\ell}^0 - n_{\mathbf{k},u}^0) e^{i\phi_{\mathbf{k}}} \\ (n_{\mathbf{k},\ell}^0 - n_{\mathbf{k},u}^0) e^{-i\phi_{\mathbf{k}}} & n_{\mathbf{k},\ell}^0 + n_{\mathbf{k},u}^0 \end{pmatrix}. \quad (5.19)$$

This leads to the following expressions for the on-site matrix of $\bar{\mathcal{P}}$ in real space, $\bar{\mathcal{P}}_{ii} \equiv \bar{P}$:

$$\bar{P}_{++} = \frac{1}{N} \sum_{\mathbf{k}} \left[\frac{n_{\mathbf{k},\ell}^0 (1 - n_{\mathbf{k},u}^0)}{2N_{\mathbf{k}s}} + \frac{n_{\mathbf{k},\ell}^0 n_{\mathbf{k},u}^0 (1 - S_-^*)}{N_{\mathbf{k}d}} \right], \quad (5.20)$$

$$\bar{P}_{+-} = \frac{1}{N} \sum_{\mathbf{k}} \left[\frac{n_{\mathbf{k},\ell}^0 (1 - n_{\mathbf{k},u}^0) e^{i\phi_{\mathbf{k}}}}{2N_{\mathbf{k}s}} + \frac{n_{\mathbf{k},\ell}^0 n_{\mathbf{k},u}^0 |R^*| e^{i\phi}}{N_{\mathbf{k}d}} \right], \quad (5.21)$$

$$\bar{P}_{--} = \frac{1}{N} \sum_{\mathbf{k}} \left[\frac{n_{\mathbf{k},\ell}^0 (1 - n_{\mathbf{k},u}^0)}{2N_{\mathbf{k}s}} + \frac{n_{\mathbf{k},\ell}^0 n_{\mathbf{k},u}^0 (1 - S_+^*)}{N_{\mathbf{k}d}} \right], \quad (5.22)$$

where the normalizing prefactor $N_{\mathbf{k}}$ depends on the occupancy of the subbands at wave vector \mathbf{k} : it equals $N_{\mathbf{k}_s}$ if only a single (viz., the lower) subband is occupied and equals $N_{\mathbf{k}_d}$ if both $|\mathbf{k}, \ell\rangle$ and $|\mathbf{k}, u\rangle$ are occupied, with

$$N_{\mathbf{k}_s} = 1 - \frac{1}{2}(S_+^* + S_-^*) - |R^*| \cos(\phi - \phi_{\mathbf{k}}), \quad (5.23)$$

$$\begin{aligned} N_{\mathbf{k}_d} &= 1 - S_+^* - S_-^* + \det S^* \\ &= (1 - S_+^*)(1 - S_-^*) - |R^*|^2. \end{aligned} \quad (5.24)$$

Setting the expressions above equal to those obtained in Eq. (4.19) one obtains a set of four equations from which to determine S_+^* , S_-^* , $|R^*|$, and ϕ .

Because of the occurrence of the phases $\phi - \phi_{\mathbf{k}}$ in Eqs. (5.20) and (5.21) these equations cannot be solved in full generality and a simplifying assumption is necessary. Thus we make here the ansatz that the off-diagonal elements of S^* vanish, i.e., $R^* = 0$. Then the terms that involve summation over the phase factors $\{\phi_{\mathbf{k}}\}$ drop out and the structure of the equations needed to determine S^* simplifies. Because the OL state is not polarized the two flavors are equivalent and the diagonal elements of S_{ii}^* must be equal, $S_+^* = S_-^* \equiv S^*$. Defining single and double occupancy in \mathbf{k} -space per \mathbf{k} point,

$$\bar{S} = \frac{1}{N} \sum_{\mathbf{k}} (1 - n_{\mathbf{k},u}) n_{\mathbf{k},\ell}, \quad (5.25)$$

$$\bar{D} = \frac{1}{N} \sum_{\mathbf{k}} n_{\mathbf{k},u} n_{\mathbf{k},\ell}, \quad (5.26)$$

one obtains a single equation for S^* in terms of \bar{S} and \bar{D} ,

$$\frac{1}{2} \frac{\bar{S}}{1 - S^*} + \frac{\bar{D}}{1 - S^*} = \frac{S^*}{1 - (S^*)^2 - g^2}. \quad (5.27)$$

Using the number of electrons per site $n = \bar{S} + 2\bar{D}$, one finds finally for the orbital liquid state

$$S^* = \frac{1}{2-n} (1 - \sqrt{1 - n(2-n)(1-g^2)}). \quad (5.28)$$

Inserting this result into the expressions for the renormalization factor and double occupancy in terms of S^* ,

$$q = 1 - \frac{S^*}{(1+g)^2} \left(1 - \frac{g^2}{1-S^*} \right), \quad (5.29)$$

$$\bar{d} = \frac{1}{2} \frac{g^2 n}{1-g^2} \frac{S^*}{1-S^*}, \quad (5.30)$$

one finally obtains

$$q(g) = 1 - \frac{1}{(1+g)^2} \frac{(1 - \sqrt{1 - n(2-n)(1-g^2)})^2}{n(2-n)}, \quad (5.31)$$

$$\bar{d}(g) = \frac{\sqrt{1 - n(2-n)(1-g^2)} + n(1-g^2) - 1}{2(1-g^2)}. \quad (5.32)$$

This expression for the kinetic energy renormalization (5.31) is identical to that which follows from Eq. (5.12) when the ordered state is unpolarized, i.e., for $q_+(g) = q_-(g) \equiv q(g)$.

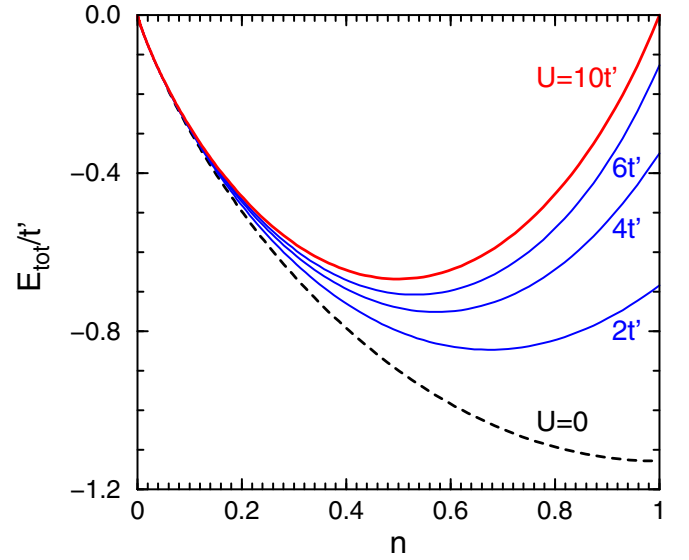


FIG. 7. Total energy E_{tot} (6.1) versus electron density n for the OL phase in the orbital e_g model with $t' \equiv t/2$. The different curves stand for $U = 0$ (black dashed line), metallic regime with $U = 2t'$, $4t'$, $6t'$ (blue solid lines), and insulating regime $U = 10t'$ (red heavy line).

At $U = \infty$ one finds $g = 0$ and

$$q(0) = \frac{1-n}{1-n/2}, \quad (5.33)$$

which reproduces the kinetic energy renormalization in the spin model.

VI. BRINKMAN-RICE TRANSITION

In the following we focus on the OL state, and in particular compare its role in the orbital Hubbard model with that of the paramagnetic phase in the spin Hubbard model. For the latter purpose it is convenient to introduce $t' \equiv t/2$; then the results obtained here at $d = \infty$ for orbital phases are directly comparable with those for magnetic phases [11].

Altogether the energy of the OL is determined by

$$E_{\text{tot}}^{\text{OL}}(n; g) = q(n; g) E_{\text{kin}}^{\text{OL}}(n) + U \bar{d}(n; g), \quad (6.1)$$

and one has to use Eqs. (5.31) and (5.32) with the optimal value of the variational parameter g . The result for the density dependence of E_{tot} for the OL phase is shown in Fig. 7 for a number of values of U . One observes that the renormalization of the kinetic energy due to electron correlations induced by U is largest at half-filling, i.e., at $n = 1$. Indeed, here one might expect an insulating state to appear eventually at sufficiently large U , with completely suppressed electron dynamics; see below. Further, with increasing U the total energy (6.1) gradually increases at any density n and its minimum moves towards $n = 0.5$. The pattern seen in Fig. 7 is entirely similar to that shown by the paramagnetic phase in the spin Hubbard model when treated likewise by the Gutzwiller method, because it is dominated by the behavior of $q(n; g)$ and $\bar{d}(n; g)$ and hardly affected by the slight difference in the shape of $E_{\text{kin}}(n)$.

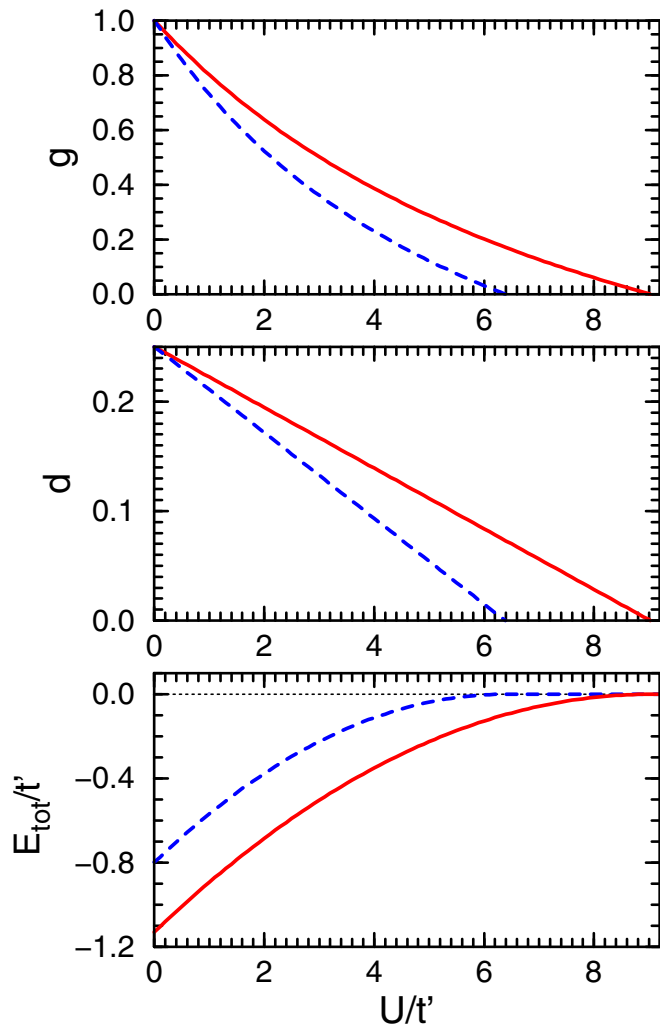


FIG. 8. Dependence on U/t' , at electron density $n = 1$, of (a) the variational parameter g , (b) the double occupancy \bar{d} , and (c) the total energy E_{tot}/t' , for the spin Hubbard model (blue dashed lines) and for the orbital e_g Hubbard model (red full lines), at $d = \infty$. For easier comparison with the spin case, we use here the hopping parameter $t' \equiv t/2$ for both spin and orbital Hubbard model.

Figure 8 shows in some more detail what happens at $n = 1$, demonstrating that for the OL in the orbital model the dependence of the variational parameter g , the double occupancy \bar{d} , and the total energy E_{tot} on U is qualitatively the same as for the paramagnetic state in the spin model. In particular double occupancy gets fully suppressed ($\bar{d} = 0$) at and above a critical value U_{BR} , while simultaneously $g = 0$ implying $q = 0$, i.e., the electrons are entirely localized and itinerancy disappears. This has been recognized in the spin case by Brinkman and Rice [91] as a qualitative criterion for the onset of the transition from a metallic to an insulating state [92], which in fact becomes exact at $d = \infty$ [93].

However, quantitatively there is a considerable difference: for the OL in the orbital e_g Hubbard model this transition occurs at $U_{\text{BR}} = 9.161 t'$, enhanced from $U_{\text{BR}} = 6.383 t'$ for the paramagnetic state in the spin Hubbard model [equivalent to the ($\gamma = 0$) POc state in the orbital model], because U_{BR} is

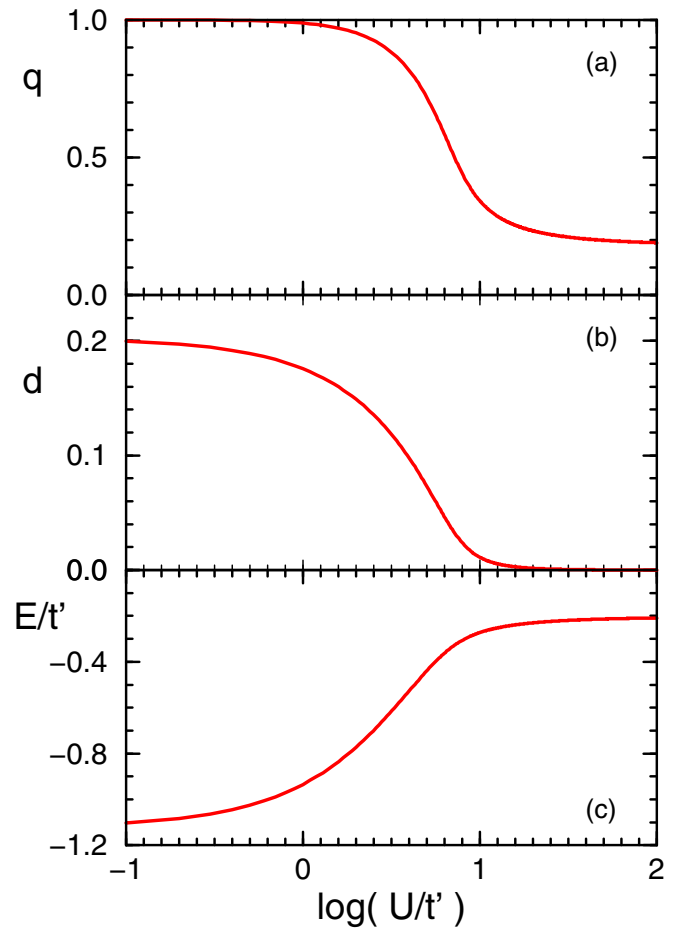


FIG. 9. Evolution of the OL phase from free electrons to a strongly correlated metal at $n = 0.9$ for increasing U/t' as obtained for the orbital e_g Hubbard model (solid lines) at $d = \infty$: (a) the Gutzwiller renormalization factor q , (b) the double occupancy \bar{d} , and (c) the total energy E_{tot} . For easier comparison with the spin case, we use here the hopping parameter $t' \equiv t/2$ for the orbital Hubbard model (2.9).

generally given by

$$U_{\text{BR}} = 8 |E_{\text{kin}}(E_{\text{F}} = 0)|, \quad (6.2)$$

which is larger by the factor $1 + \sqrt{\pi}F(1; 0) = 1.435$ for the OL; compare Eqs. (3.37) and (3.29). Clearly this is entirely due to the extra contribution to the kinetic energy coming from the orbital-flavor nonconserving hopping at $\gamma = 1$. We note in passing that the real para-orbital phase PO_r shows a Brinkman-Rice transition at the intermediate value $U_{\text{BR}} = 7.818 t'$, enhanced only by a factor $w_r/w_c = \sigma(\gamma = 1) = \sqrt{3/2} = 1.225$, because it profits only partially from the additional kinetic energy available in the orbital model.

At $n < 1$ the renormalization factor $q(g)$, Eq. (5.31), remains finite at large U , and thus the electrons remain itinerant, but with reduced kinetic energy; see Fig. 9. Increasing U/t' defines here three distinct regimes:

- (i) at very small U ($U \lesssim t'$) correlations are virtually absent, $q \approx 1$ and $\bar{d} \approx (n/2)^2$,
- (ii) at small U ($U < U_{\text{BR}}$) the correlations gradually develop, $q(g)$ is reduced from 1.0 down to ≈ 0.2 , double

occupancy is strongly reduced ($\bar{d} \rightarrow 0$), and the total energy increases, and

(iii) at large U ($U > U_{BR}$) the correlations dominate, double occupancy becomes excluded, and the electrons move in the strongly correlated OL without creating double occupancies.

VII. PHASE DIAGRAM

From the unrenormalized kinetic energies shown in Fig. 6 we concluded that the uniformly polarized FOr phase and possibly the disordered POr phase are the only candidates competing with the OL phase for being the ground state after the energies of the POr and OL phase have been renormalized by correlations, for the following reasons: First, as double occupancies do not occur in the FOr phase or the other uniform phases with broken symmetry, these phases are not affected by renormalization and so the sequence of their energies is fixed. Second, although the energies of the disordered phases are changed by accounting for correlations, their sequential order also cannot change if all of them are subjected to the same renormalization procedure (at least if the procedure is only sensitive to energies as is the case for the Gutzwiller method). This holds because for any phase its total renormalized energy is given by an expression like Eq. (6.1) with the variational parameter(s) optimized for the lowest outcome; if the kinetic energy in this equation is replaced by a lower value associated with a different phase, the total energy is lowered even if the variational parameter g is kept fixed; subsequently allowing g to optimize can only lead to a further lowering of the total energy. This argument should not only hold for the para-orbital phases but also be valid between the POr and OL phases, implying that the only competition of interest should be between the FOr phase and the OL phase.

Numerical results are shown in Fig. 10(a) for the dependence upon density of the total energies of various phases at a particular value of U , viz., $U = 10t$. The states other than the FOr and the OL states are included here just to demonstrate that they do not play a role, as argued above. Yet, indeed, a competition between the FOr phase and the OL does take place and the total energies of these phases are seen to be quite close to one another. In fact they cross and, whereas the energy of the OL is well below that of the FOr state over most of the density range even for this rather large value of U , the OL phase is unstable against the FOr phase close to $n = 1$, as shown in more detail in Fig. 10(b). We point out that the latter result is different from that obtained for the 3D orbital Hubbard model (at $d = 3$), where the OL is stable in the entire regime of n also at large U [13].

The transition between the OL phase and the FOr phase can be determined more accurately by calculating at fixed n the total energy of the OL as a function of U and comparing this with the U independent total energy of the FOr state, as shown in Fig. 11. One thus obtains $U_c(n)$ where the two phases have equal energy. This defines the OL-FOr phase boundary because the transition is first order, since the states $|\Psi^{OL}\rangle$ and $|\Psi^{FOr}\rangle$ cannot transform continuously into one another because of the globally different structure of $|\Phi_0^{OL}\rangle$ and $|\Phi_0^{FOr}\rangle$. This stands in clear contrast to the paramagnetic-ferromagnetic transition in the spin Hubbard model, which is second order because the magnetization can evolve gradually from the paramagnetic state.

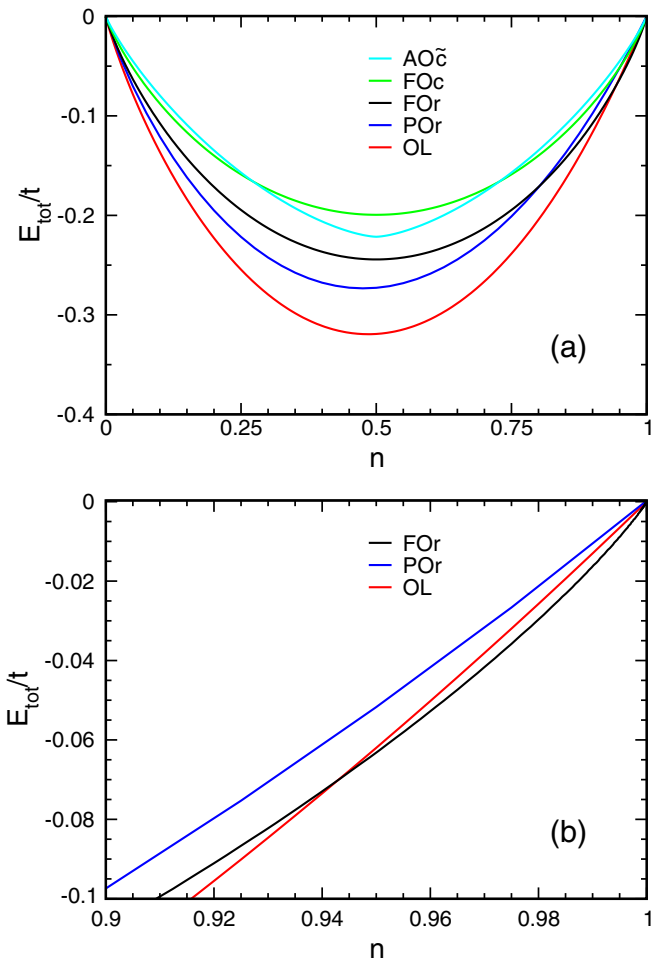


FIG. 10. Total energy E_{tot} as a function of density n at $U = 10t$ for the OL state (red line), the real-orbital POr state (blue line), the real-orbital FOr state (black line), the complex-orbital FOC state (green line), and the phased complex-orbital AO \check{c} state (cyan line): (a) for OL, POr, FOr, FOC, and AO \check{c} in the range $0 \leq n \leq 1$; (b) zoom-in on the range close to $n = 1$ for OL, POr, and FOr only.

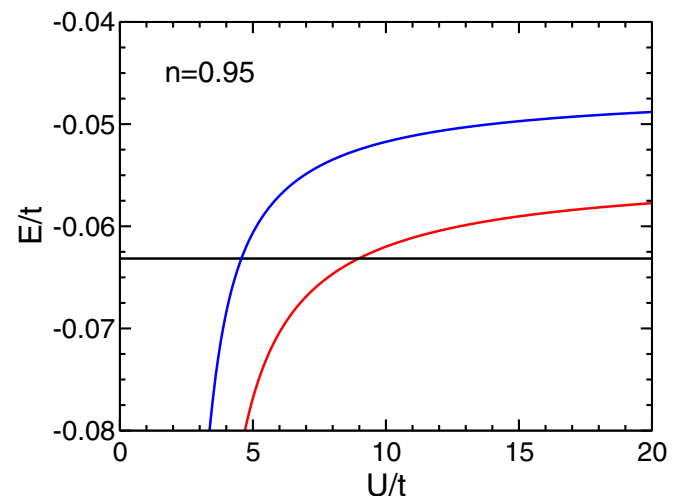


FIG. 11. Total energy E_{tot} as a function of the Hubbard interaction parameter U/t for the OL phase (red line), real-orbital FOr state (black horizontal line, independent of U), and real-orbital POr state (blue line) for fixed $n = 0.95$.

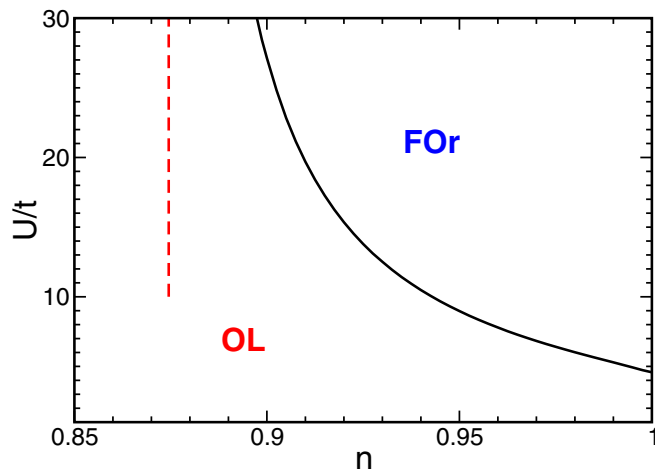


FIG. 12. Phase diagram of the OL state versus the FOr state at $d = \infty$. The FOr phase is more stable than the OL phase for $U > U_c(n)$ if $n > n_c$. The vertical red dashed line indicates the phase boundary for $U = \infty$ at n_c ; $U_c(1) = 4.5805t$ is equal to the critical value of the interaction for the Brinkman-Rice transition [91] in the OL state.

The resulting phase diagram of the orbital e_g Hubbard model in the (n, U) plane as obtained in the Gutzwiller approximation is shown in Fig. 12. The FOr phase is more stable than the OL phase for $U > U_c(n)$ if $n > n_c$. Here $n_c = 0.8746$ is the critical value of the particle density at which the energies of the phases are equal at $U = \infty$, and below which the OL is therefore always stable; see Fig. 12. It is obtained from a numerical comparison using the analytical expressions for the kinetic energies of the two phases, Eqs. (3.31) and (3.37), and for the renormalization factor at $U = \infty$, Eq. (5.33).

Next we consider the intersection of the phase boundary with the U/t axis at $n = 1$. With our simple representation of real ferro-orbital order by the state $|\Psi^{\text{FOr}}\rangle = |\Phi_0^{\text{FOr}}\rangle$, which has fully saturated orbital order such that $E_{\text{tot}}^{\text{FOr}}(1) = E_{\text{kin}}^{\text{FOr}}(1) = 0$ independent of U , this intersection necessarily coincides with the Brinkman-Rice transition point where the energy of the OL attains 0, so $U_c(1) = U_{\text{BR}} = 4.5805t$. However, as pointed out by Fazekas *et al.* for the spin case [11], precisely close to $n = 1$ a small reduction of the polarization must occur involving the exponential tails of the DOSs of the x_0 and \bar{x}_0 bands. If this would be taken into account it would produce some lowering of the energy of the FOr phase thus leading to a slight decrease of $U_c(1)$.

Allowing some polarization of the FOr state at general density, at the price of creating double occupancy, would similarly give some energy lowering. However, this is severely limited by the restriction that upon transferring one particle from the majority to the minority band the gain in kinetic energy must exceed U . This condition is only met as long as the Fermi energy of the minority band is in the exponential tail of the DOS, i.e., only for a very small fraction of the particles, and also $U \lesssim 4t$; compare Fig. 2(b). Thus our use of the fully ordered state $|\Psi^{\text{FOr}}\rangle$ neglects at most a minor expansion of the FOr regime in the phase diagram.

We have not attempted to construct a more sophisticated trial state for any of the AO phases, such as has been shown to be important to obtain a good description of the AF phase in the spin Hubbard model [8,11]. So, strictly we cannot

exclude that alternating orbital order would show up in the orbital model at and/or close to half-filling by outcompeting the ferro-orbital order, as occurs between antiferromagnetism and ferromagnetism in the spin case. However, this seems unlikely in the orbital case because of the large difference in kinetic energy between the fully ordered states (see Fig. 6), viz., by a factor $w_r/w_{r,\text{ao}} = \sigma\sqrt{2} = \sqrt{3} = 1.73$ between the FOr and AOr states, and (because the kinetic energy of the AO \check{c} state is very close to that of the FOC state) by a factor $\simeq w_r/w_c = \sigma = \sqrt{3/2} = 1.22$ between the FOr and AO \check{c} states. As shown above, this difference is due to the more efficient use of both pseudospin-conserving and -nonconserving hopping channels by real ferro-orbital order than by alternating orbital order. What we have established is that the OL state is the ground state over most of the (n, U) phase diagram, as illustrated by Fig. 12.

Finally, we point out that the phase diagram obtained here at $d = \infty$ is qualitatively different from that found before at $d = 3$ [13]. In the latter case the lowest-energy ordered FOx phase was completely eliminated from the phase diagram by the nonconserving hopping, and the OL phase was the only phase present. We propose that this is caused by the different energy ranges: $[-3t, 3t]$ at $d = 3$ versus $[-\infty, \infty]$ at $d = \infty$. The argumentation is as follows:

Let us consider, at $U = \infty$, the derivatives with respect to n of the total energy of the candidate phases (viz. FOr and OL at $d = \infty$, FOx and OL at $d = 3$) at $n = 1$, as these determine which phase has the lowest energy in the immediate vicinity of half-filling; compare Fig. 10. Since $\bar{d} = 0$ at $U = \infty$, we have $E_{\text{tot}}^{\text{FO}}(n) = E_{\text{kin}}^{\text{FO}}(n)$ and $E_{\text{tot}}^{\text{OL}}(n) = q(n)E_{\text{kin}}^{\text{OL}}(n)$ [compare Eq. (6.1)], and therefore

$$\frac{dE_{\text{tot}}^{\text{FO}}(n)}{dn} = \frac{dE_{\text{kin}}^{\text{FO}}(n)}{dn} = E_{\text{F}}^{\text{FO}}(n), \quad (7.1)$$

$$\begin{aligned} \frac{dE_{\text{tot}}^{\text{OL}}(n)}{dn} &= \frac{dq}{dn}(n)E_{\text{kin}}^{\text{OL}}(n) + q(n)\frac{dE_{\text{kin}}^{\text{OL}}(n)}{dn} \\ &= \frac{dq}{dn}(n)E_{\text{kin}}^{\text{OL}}(n) + q(n)E_{\text{F}}^{\text{OL}}(n). \end{aligned} \quad (7.2)$$

Both expressions can be evaluated,

(i) at $d = 3$: by consulting [13], for the FOx phase using Eq. (3.23) therein (from which one obtains $E_{\text{kin}}^{\text{FOx}}(1-x) \simeq 3t(1-x + \dots)$ and thus $E_{\text{F}}^{\text{FOx}}(1) = 3t$), for the OL phase making use of the data plotted in Fig. 5 therein [from which one obtains $E_{\text{kin}}^{\text{OL}}(1) \simeq -1.52t$ and $E_{\text{F}}^{\text{OL}}(1) = 0$];

(ii) at $d = \infty$: for the FOr phase using Eqs. (3.30) in the present paper with $w_r = \sqrt{3/2}/2$, for the OL phase using Eq. (3.37) and so obtaining $E_{\text{kin}}^{\text{OL}}(1) \simeq -0.5726t$;

(iii) inserting $q(1) = 0$ and $dq/dn(1) = -2$.

The results are as follows:

$$d = 3 : \frac{dE_{\text{tot}}^{\text{FOx}}}{dn}(1) = 3.00t, \quad (7.3)$$

$$d = 3 : \frac{dE_{\text{tot}}^{\text{OL}}}{dn}(1) = 3.04t, \quad (7.4)$$

$$d = \infty : \frac{dE_{\text{tot}}^{\text{FOr}}}{dn}(1-x) = 0.8660 \operatorname{inverf}(1-2x)t, \quad (7.5)$$

$$d = \infty : \frac{dE_{\text{tot}}^{\text{OL}}}{dn}(1) = 1.1451t. \quad (7.6)$$

So, for $d = 3$ the derivative is slightly larger for the OL, implying that close to $n = 1$ this is the lowest state and then will remain so in the entire phase diagram, as we found before [13]. However, for $d = \infty$ the slope for the FOr phase initially diverges [the function $\text{inverf}(y) \rightarrow \infty$ at $y \rightarrow 1$], so the FOr state is the ground state close to $n = 1$, as we found in the present paper. This divergence is not seen in the plots because it is very steep. Thus already for $x = 1 - n$ larger than 0.03 the derivative is of order 1 and with further increasing x the FOr phase begins to be overtaken by the OL. So the reason for the FOr phase being stable at $d = \infty$ apparently lies in the exponential tails in its DOS, particle density, and kinetic energy. As this is a mathematical rather than a physical phenomenon, the above result suggests that stability of ordered phases at $d = \infty$ is mathematically correct but physically spurious, and that the earlier theoretical result at $d = 3$ [13] describes the generic physics.

We thus conclude that regarding the phase diagram the $d = \infty$ case is not representative for all dimensions: the $d = 3$ case is qualitatively different. This actually demonstrates that the effect of the nonconserving hopping terms themselves is qualitatively different for different dimensions, which is not the case for the conserving terms, since FM and AF phases appear in the phase diagram of the spin Hubbard model in all dimensions.

VIII. DISCUSSION AND CONCLUSIONS

A. General aspects of the $d = \infty$ orbital model

A few aspects of the e_g orbital Hubbard model at $d = \infty$ deserve some further comments. They mainly concern the limitations of the Gutzwiller approach in comparison with more powerful recent methods, in particular self-consistent DMFT. As mentioned briefly in Sec. I, the development of the DMFT approach [62] was made possible by the discovery by Metzner and Vollhardt that in the limit $d = \infty$ only on-site correlations survive [8]. Nowadays DMFT is recognized as a standard method to study electron correlation effects in the electronic structure [94–97]. This method has been successfully applied, *inter alia*, to the Falicov-Kimball model [98] and to nonequilibrium dynamics [99]. The ideas employed using the Gutzwiller wave function helped to formulate the DMFT method in spin systems [95].

First of all, one may wonder to what extent the description of the metal-insulator transition, as presented in Sec. VI, i.e., as a Brinkman-Rice transition, is realistic. An additional aspect for the orbital model is possible crystal-field splittings, but it has been established that orbital-selective Mott phases occur then for large enough interaction U [100,101]. However, when the orbitals remain equivalent, as in the OL state considered in the present paper, one may expect that the transition occurs in a similar way as in the paramagnetic state in the spin model. So our treatment of the metal-insulator transition in the orbital model at $d = \infty$ by the Gutzwiller approach, leading to the Brinkman-Rice transition, then has the same status as the treatment of the metal-insulator transition in the spin model at $d = \infty$ by that same approach, and gives valuable insight how correlations induce the system to approach the localized state [95].

Second, past calculations using the Gutzwiller wave function have led to a better understanding of the strongly correlated regime of the Hubbard model. In one dimension the metal-insulator transition is absent but several quantities have been calculated exactly [102]: the double occupation, the momentum distribution, as well as its discontinuity at the Fermi surface. These quantities determine the expectation value of the 1D Hubbard Hamiltonian for any symmetric and monotonically increasing dispersion. The Gutzwiller wave function has also been found to predict ferromagnetic behavior for sufficiently large interaction U [103,104]. This agrees with the present result that the orbital Hubbard model also has a range of ferro-orbital states close to $n = 1$.

However, it has been known for some time that the Brinkman-Rice picture of the metal-insulator transition, as given by the Gutzwiller approach both at $d = 3$ and at $d = \infty$, is oversimplified, in particular yielding a poor description of the dynamics on the insulating side [105]. Recent studies of the metal-insulator transition in the spin Hubbard model at $d = \infty$ by DMFT have demonstrated the existence of two different transitions—a metal-to-insulator transition at U_{c2} where the quasiparticle weight becomes zero and an insulator-to-metal transition at U_{c1} where the gap closes, both first-order—and the occurrence of hysteresis between the two critical interaction strengths [106–108]. This holds from $T = 0$ up to a critical temperature T_c , where U_{c1} and U_{c2} coalesce, while for $T > T_c$ there is a smooth crossover between metallic and insulating behavior. Notably, the thermodynamics of the hysteresis region was recently explained at the two-particle level [109]. Obviously, the above more-detailed understanding of the Mott-Hubbard transition implies that this transition is considerably more complex than the Brinkman-Rice picture suggests.

These differences between the Mott-Hubbard transition in the spin Hubbard model as calculated by DMFT and the Brinkman-Rice picture are clearly due to the fact that DMFT is coping more effectively with correlations than the Gutzwiller approach. One would therefore expect that a DMFT treatment of the e_g orbital Hubbard model would produce similar changes to the metal-insulator transition as in the spin Hubbard model, because this transition is typically a correlation-induced phenomenon. By contrast, one would expect the more prominent role of the disordered OL in the phase diagram (as compared to the paramagnetic phase in the spin case) to remain largely unaffected, because it is not due to correlations but to the additional kinetic energy provided by the nonconserving hopping channel.

However, these are just speculations. We emphasize that orbital models such as that in Eq. (2.9) [or Eq. (2.7)] have as yet not been studied in the context of self-consistent DMFT calculations. Therefore, even the corresponding effective impurity model for such calculations is not known, and its construction appears not to be entirely trivial. A prime candidate is a two-orbital Anderson impurity model with on-site U and self-consistently generated orbital flipping terms. In view of the overriding importance of the orbital nonconserving hopping channel and the associated C_d symmetry demonstrated above, these features should apparently be incorporated somehow. The only way seems to be by imposing a specific structure on the bath modes and their coupling to the impurity. It would be desirable

if a DMFT treatment along these lines were performed, both to see if the above speculations on the e_g orbital Hubbard model are born out and to further explore the application of the DMFT method to a wider range of models.

The early ideas of Kugel and Khomskii [19] culminate in systems where spins and orbitals become almost equivalent. This idealization happens for face-sharing octahedra and one finds indeed a highly symmetric SU(4) model [110]. So far, studies of such systems have only been performed theoretically and these have identified an interesting evolution of spin-orbital entanglement with increasing spin-orbit coupling [66]. In spite of the absence of long-range spin-orbital order such systems exhibit features typical of those manifesting themselves at phase transitions [111]. The experimental search for quantum spin-orbital liquids identified FeSc₂S₄ as a quantum material with long-range entanglement [112]. Such states are primarily realized in the Kitaev materials where spins and orbitals lose their identity and are strongly entangled by large spin-orbit coupling [113]. The challenge in the theory is to find a quantum spin-orbital liquid at infinite dimension.

B. Summary

Summarizing, we have presented a generalization of the e_g orbital model to infinite dimension $d = \infty$, preserving the twofold degeneracy of the orbitals and turning the lattice symmetry from cubic into hypercubic. It is quite remarkable that the two-flavor orbital model is manifestly different from the corresponding spin model at $d = \infty$ by the presence of orbital-flipping hopping terms. At the same time it is somewhat surprising that the two orbital flavors are equivalent in the limit of $d = \infty$ when they are so different in the 3D model, including the physics of the manganites [80]. We have further shown that the Gutzwiller approximation becomes exact in the limit $d \rightarrow \infty$ for the orbital Hubbard model, in perfect analogy with the spin Hubbard model.

We conclude that the peculiar features of the orbital Hubbard model (2.9) are due to the fact that the extra hopping terms $\propto \gamma t$ do not conserve the pseudospin as they mix the two orbital flavors. They thus induce the following distinctive features:

(i) There are two classes of single-particle plane-wave states: those with complex orbitals and those with real orbitals, which behave differently. The same holds for the Fermi-sea-like multiparticle states built from them.

(ii) The single-particle *eigenstates* of the kinetic energy form two distinct bands with different dispersions.

(iii) Each such eigenstate carries a nonzero polarization, i.e., contributes to the pseudospin at all sites. Yet, when summed over all eigenstates in an energy shell, these contributions add up to zero. By this mechanism the *orbital liquid state* (OL), which is obtained by filling the two bands of single-particle eigenstates to the same Fermi energy, is unpolarized at any filling.

The above qualitative features are generic for the e_g orbital Hubbard model, i.e., they hold at any dimension, from $d = 3$ up to $d = \infty$.

There are also a number of features induced by the nonconserving hopping channel that are to some extent quantitative and are most pronounced at $d = \infty$.

(iv) The extra hopping channel lowers the kinetic energy with respect to the spin case and thus makes the Brinkman-Rice transition to an insulator occur at a larger value of U .

(v.a) Phases with alternating orbitals are much less favored than antiferromagnetism for fermions on a bipartite lattice like the hypercubic lattices considered here, because they benefit relatively less from the pseudospin-conserving channel, whereas

(v.b) unlike ferromagnetic states in the spin Hubbard model, ferro-orbital states are not eigenstates of the orbital Hubbard model (2.9) and benefit energetically more from the orbital-mixing term.

(v.c) Together this makes the FOr state the main competitor of the orbital liquid phase, and the $d = \infty$ phase diagram confirms that FOr order indeed occurs at large U close to half-filling [114], while the orbital liquid phase is the ground state elsewhere.

(v.d) The stability of the FOr is apparently due to the exponential tails in the DOS, particle density and kinetic energy, and so is specific for $d = \infty$, whereas at $d = 3$ the OL phase is the lowest-energy state in the entire phase diagram.

Perhaps feature (v.a) is the most remarkable quantitative consequence of orbital physics. Having richer hopping processes both with and without the restriction that the orbital flavor is conserved, one has to accept that alternating orbital order is more difficult to realize than in the spin model [11]. Feature (v.b) makes it more difficult to realize fully polarized ferro-orbital states, so it may sound surprising that nevertheless the FOr phase is more stable than the orbital liquid in a range of electron densities $n \geq n_c$. Note that the theorem formulated by Nagaoka [115] at $U = \infty$ for the spin case does not apply to the orbital Hubbard model.

One of the attractive ideas in this field has been the possible existence of polarized ferro-orbital states with partly filled *complex* orbitals [116]. We have established that unfortunately such states cannot be realized. We have shown that they are unstable and one has to consider instead FOr states.

ACKNOWLEDGMENTS

We thank Walter Metzner for his interest and for very insightful discussions. L.F.F. thanks the Max Planck Institute for Solid State Research in Stuttgart and the Jagiellonian University in Kraków for their kind hospitality. A.M.O. kindly acknowledges Narodowe Centrum Nauki (NCN, Poland) Project No. 2016/23/B/ST3/00839 and is grateful for support via the Alexander von Humboldt Foundation Fellowship (Humboldt-Forschungspreis) [117].

APPENDIX: PROOF THAT THE ORBITAL LIQUID PHASE IS UNPOLARIZED

Consider the cyclic permutation C defined by

$$\begin{aligned} \mathbf{C}k &= \mathbf{C}(k_{-m}, k_{-m+1}, \dots, k_0, \dots, k_m) \\ &\equiv (k_m, k_{-m}, \dots, k_{-1}, \dots, k_{m-1}). \end{aligned} \quad (\text{A1})$$

Then we have [compare Eqs. (2.15) and (2.16)]

$$\begin{aligned}
 G_{\mathbf{Ck}} &= B_{\mathbf{Ck}} \exp(i\phi_{\mathbf{Ck}}) = \sum_n \cos(\mathbf{Ck})_n e^{i\chi_n} \\
 &= \sum_n \cos k_{n-1} e^{i\chi_n} = \sum_n \cos k_n e^{i\chi_{n+1}} \\
 &= e^{i4\pi/d} G_{\mathbf{k}} = B_{\mathbf{k}} e^{i4\pi/d} \exp(i\phi_{\mathbf{k}}), \quad (\text{A2})
 \end{aligned}$$

and it follows that $B_{\mathbf{Ck}} = B_{\mathbf{k}}$ and $\phi_{\mathbf{Ck}} = \phi_{\mathbf{k}} + 4\pi/d$. The set of \mathbf{k} vectors generated from \mathbf{k} by successive permutations is $\Pi(\mathbf{k}) = \{\mathbf{C}^n \mathbf{k} \mid -m \leq n \leq m\}$, so

$$\begin{aligned}
 \sum_{\mathbf{k}' \in \Pi(\mathbf{k})} e^{i\phi_{\mathbf{k}'}} &= \sum_n \exp(i\phi_{\mathbf{C}^n \mathbf{k}}) = \sum_n \exp[i(\phi_{\mathbf{k}} + 4n\pi/d)] \\
 &= e^{i\phi_{\mathbf{k}}} \sum_n e^{i4n\pi/d} = e^{i\phi_{\mathbf{k}}} \sum_n e^{i\chi_n} = 0. \quad (\text{A3})
 \end{aligned}$$

-
- [1] J. Hubbard, Electron correlations in narrow energy bands, *Proc. R. Soc. London A* **276**, 238 (1963).
- [2] P. W. Anderson, New approach to the theory of superexchange interactions, *Phys. Rev.* **115**, 2 (1959).
- [3] W. Metzner and D. Vollhardt, Correlated Lattice Fermions in $d = \infty$ Dimension, *Phys. Rev. Lett.* **62**, 324 (1989).
- [4] W. Metzner and D. Vollhardt, Analytic calculation of ground-state properties of correlated fermions with the Gutzwiller wave-function, *Phys. Rev. B* **37**, 7382 (1988).
- [5] M. C. Gutzwiller, Effect of Correlation on the Ferromagnetism of Transition Metals, *Phys. Rev. Lett.* **10**, 159 (1963).
- [6] M. C. Gutzwiller, Correlation of electrons in a narrow s band, *Phys. Rev.* **137**, A1726 (1965).
- [7] D. Vollhardt, Normal He^3 : An almost localized Fermi liquid, *Rev. Mod. Phys.* **56**, 99 (1984).
- [8] W. Metzner, Variational theory for correlated lattice fermions in high dimension, *Z. Phys. B* **77**, 253 (1989).
- [9] W. Metzner, Analytic evaluation of resonating valence bond states, *Z. Phys. B* **82**, 183 (1991).
- [10] P. W. Anderson, Resonating valence bonds: A new kind of insulator?, *Mater. Res. Bull.* **8**, 153 (1973).
- [11] P. Fazekas, B. Menge, and E. Müller-Hartmann, Ground state phase diagram of the infinite dimensional Hubbard model: A variational study, *Z. Phys. B* **78**, 69 (1990).
- [12] S. Ishihara, M. Yamanaka, and N. Nagaosa, Orbital liquid in perovskite transition-metal oxides, *Phys. Rev. B* **56**, 686 (1997).
- [13] L. F. Feiner and A. M. Oleś, Orbital liquid in ferromagnetic manganites: The orbital Hubbard model for e_g electrons, *Phys. Rev. B* **71**, 144422 (2005).
- [14] T. Tanaka, M. Matsumoto, and S. Ishihara, Randomly Diluted e_g Orbital-Ordered Systems, *Phys. Rev. Lett.* **95**, 267204 (2005).
- [15] T. Tanaka and S. Ishihara, Dilution Effects in Two-Dimensional Quantum Orbital Systems, *Phys. Rev. Lett.* **98**, 256402 (2007).
- [16] P. Czarnik, J. Dziarmaga, and A. M. Oleś, Overcoming the sign problem at finite temperature: Quantum tensor network for the orbital e_g model on an infinite square lattice, *Phys. Rev. B* **96**, 014420 (2017).
- [17] L. Balents, Spin liquids in frustrated magnets, *Nature (London)* **464**, 199 (2010).
- [18] L. Savary and L. Balents, Quantum spin liquids: A review, *Rep. Prog. Phys.* **80**, 016502 (2017).
- [19] K. I. Kugel and D. I. Khomskii, The Jahn-Teller effect and magnetism: Transition metal compounds, *Usp. Fiz. Nauk* **136**, 621 (1982) [*Sov. Phys. Usp.* **25**, 231 (1982)].
- [20] D. I. Khomskii, *Transition Metal Oxides* (Cambridge University Press, Cambridge, 2014).
- [21] M. Imada, A. Fujimori, and Y. Tokura, Metal-insulator transitions, *Rev. Mod. Phys.* **70**, 1039 (1998).
- [22] Y. Tokura and N. Nagaosa, Orbital physics in transition-metal oxides, *Science* **288**, 462 (2000).
- [23] A. V. Gorshkov, M. Hermele, V. Gurarie, C. Xu, P. S. Julienne, J. Ye, P. Zoller, E. Demler, M. D. Lukin, and A. M. Rey, Two-orbital $\text{SU}(N)$ magnetism with ultracold alkaline-earth atoms, *Nat. Phys.* **6**, 289 (2010).
- [24] A. Koga, N. Kawakami, T. M. Rice, and M. Sigrist, Orbital-Selective Mott Transitions in the Degenerate Hubbard Model, *Phys. Rev. Lett.* **92**, 216402 (2004).
- [25] L. F. Feiner, A. M. Oleś, and J. Zaanen, Quantum Melting of Magnetic Order due to Orbital Fluctuations, *Phys. Rev. Lett.* **78**, 2799 (1997).
- [26] L. F. Feiner, A. M. Oleś, and J. Zaanen, Quantum disorder versus order-out-of-order in the Kugel-Khomskii model, *J. Phys.: Condens. Matter* **10**, L555 (1998).
- [27] G. Khaliullin and V. Oudovenko, Spin and orbital excitation spectrum in the Kugel-Khomskii model, *Phys. Rev. B* **56**, R14243 (1997).
- [28] P. Corboz, M. Lajkó, A. M. Läuchli, K. Penc, and F. Mila, Spin-Orbital Quantum Liquid on the Honeycomb Lattice, *Phys. Rev. X* **2**, 041013 (2012).
- [29] G. Khaliullin and S. Maekawa, Orbital Liquid in Three-Dimensional Mott Insulator: LaTiO_3 , *Phys. Rev. Lett.* **85**, 3950 (2000).
- [30] G. Khaliullin, Orbital order and fluctuations in Mott insulators, *Prog. Theor. Phys. Suppl.* **160**, 155 (2005).
- [31] K. Kitagawa, T. Takayama, Y. Matsumoto, A. Kato, R. Takano, Y. Kishimoto, S. Bette, R. Dinnebier, G. Jackeli, and H. Takagi, A spin-orbital-entangled quantum liquid on a honeycomb lattice, *Nature (London)* **554**, 341 (2018).
- [32] L. F. Feiner and A. M. Oleś, Electronic origin of magnetic and orbital ordering in insulating LaMnO_3 , *Phys. Rev. B* **59**, 3295 (1999).
- [33] J. van den Brink, P. Horsch, F. Mack, and A. M. Oleś, Orbital dynamics in ferromagnetic transition-metal oxides, *Phys. Rev. B* **59**, 6795 (1999).
- [34] A. M. Oleś, G. Khaliullin, P. Horsch, and L. F. Feiner, Fingerprints of spin-orbital physics in cubic Mott insulators: Magnetic exchange interactions and optical spectral weights, *Phys. Rev. B* **72**, 214431 (2005).
- [35] A. Reitsma, L. F. Feiner, and A. M. Oleś, Orbital and spin physics in LiNiO_2 and NaNiO_2 , *New J. Phys.* **7**, 121 (2005).

- [36] J. Chaloupka and G. Khaliullin, Orbital Order and Possible Superconductivity in $\text{LaNiO}_3/\text{LaMO}_3$ Superlattices, *Phys. Rev. Lett.* **100**, 016404 (2008).
- [37] V. I. Solovyeu, Spin-orbital superexchange physics emerging from interacting oxygen molecules in KO_2 , *New J. Phys.* **10**, 013035 (2008).
- [38] B. Normand and A. M. Oleś, Frustration and entanglement in the t_{2g} spin-orbital model on a triangular lattice: Valence-bond and generalized liquid states, *Phys. Rev. B* **78**, 094427 (2008).
- [39] F. Krüger, S. Kumar, J. Zaanen, and J. van den Brink, Spin-orbital frustrations and anomalous metallic state in iron-pnictide superconductors, *Phys. Rev. B* **79**, 054504 (2009).
- [40] W. Lv, F. Krüger, and P. Phillips, Orbital ordering and unfrustrated $(\pi, 0)$ magnetism from degenerate double exchange in the iron pnictides, *Phys. Rev. B* **82**, 045125 (2010).
- [41] B. Normand, Multicolored quantum dimer models, resonating valence-bond states, color visons, and the triangular-lattice t_{2g} spin-orbital system, *Phys. Rev. B* **83**, 064413 (2011).
- [42] J. Chaloupka and A. M. Oleś, Spin-orbital resonating valence-bond liquid on a triangular lattice: Evidence from finite cluster diagonalization, *Phys. Rev. B* **83**, 094406 (2011).
- [43] K. Wohlfeld, M. Daghofer, and A. M. Oleś, Spin-orbital physics for p orbitals in alkali hyperoxides—Generalization of the Goodenough-Kanamori rules, *Europhys. Lett.* **96**, 27001 (2011).
- [44] K. Wohlfeld, M. Daghofer, S. Nishimoto, G. Khaliullin, and J. van den Brink, Intrinsic Coupling of Orbital Excitations to Spin Fluctuations in Mott Insulators, *Phys. Rev. Lett.* **107**, 147201 (2011).
- [45] J. Schlappa, K. Wohlfeld, K. J. Zhou, M. Mourigal, M. W. Haverkort, V. N. Strocov, L. Hozoi, C. Monney, S. Nishimoto, S. Singh, A. Revcolevschi, J.-S. Caux, L. Patthey, H. M. Ronnow, J. van den Brink, and T. Schmitt, Spin-orbital separation in the quasi-one-dimensional Mott insulator Sr_2CuO_3 , *Nature (London)* **485**, 82 (2012).
- [46] K. Wohlfeld, S. Nishimoto, M. W. Haverkort, and J. van den Brink, Microscopic origin of spin-orbital separation in Sr_2CuO_3 , *Phys. Rev. B* **88**, 195138 (2013).
- [47] V. Bisogni, K. Wohlfeld, S. Nishimoto, C. Monney, J. Trinckauf, K. Zhou, R. Kraus, K. Koepf, C. Sekar, V. Strocov, B. Büchner, T. Schmitt, J. van den Brink, and J. Geck, Orbital Control of Effective Dimensionality: From Spin-Orbital Fractionalization to Confinement in the Anisotropic Ladder System CaCu_2O_3 , *Phys. Rev. Lett.* **114**, 096402 (2015).
- [48] C.-C. Chen, M. van Veenendaal, T. P. Devereaux, and K. Wohlfeld, Fractionalization, entanglement, and separation: Understanding the collective excitations in a spin-orbital chain, *Phys. Rev. B* **91**, 165102 (2015).
- [49] W. Brzezicki, A. M. Oleś, and M. Cuoco, Spin-Orbital Order Modified by Orbital Dilution in Transition-Metal Oxides: From Spin Defects to Frustrated Spins Polarizing Host Orbitals, *Phys. Rev. X* **5**, 011037 (2015).
- [50] W. Brzezicki, M. Cuoco, and A. M. Oleś, Novel spin-orbital phases induced by orbital dilution, *J. Supercond. Novel Magn.* **29**, 563 (2016).
- [51] W. Brzezicki, M. Cuoco, and A. M. Oleś, Exotic spin-orbital physics in hybrid oxides, *J. Supercond. Novel Magn.* **30**, 129 (2017).
- [52] J. B. Goodenough, *Magnetism and the Chemical Bond* (Interscience, New York, 1963).
- [53] A. M. Oleś, P. Horsch, L. F. Feiner, and G. Khaliullin, Spin-Orbital Entanglement and Violation of the Goodenough-Kanamori Rules, *Phys. Rev. Lett.* **96**, 147205 (2006).
- [54] A. M. Oleś, Fingerprints of spin-orbital entanglement in transition metal oxides, *J. Phys.: Condens. Matter* **24**, 313201 (2012).
- [55] W. Brzezicki, J. Dziarmaga, and A. M. Oleś, Noncollinear Magnetic Order Stabilized by Entangled Spin-Orbital Fluctuations, *Phys. Rev. Lett.* **109**, 237201 (2012).
- [56] W. Brzezicki, J. Dziarmaga, and A. M. Oleś, Exotic spin orders driven by orbital fluctuations in the Kugel-Khomskii model, *Phys. Rev. B* **87**, 064407 (2013).
- [57] M. Snamina and A. M. Oleś, Magnon dressing by orbital excitations in ferromagnetic planes of K_2CuF_4 and LaMnO_3 , *New J. Phys.* **21**, 023018 (2019).
- [58] W. Brzezicki, Spin, orbital and topological order in models of strongly correlated electrons, *J. Phys.: Condens. Matter* **32**, 023001 (2020).
- [59] P. A. Lee, N. Nagaosa, and X.-G. Wen, Doping a Mott insulator: Physics of high-temperature superconductivity, *Rev. Mod. Phys.* **78**, 17 (2006).
- [60] M. Ogata and H. Fukuyama, The t - J model for the oxide high- T_c superconductors, *Rep. Prog. Phys.* **71**, 036501 (2008).
- [61] B. Keimer, S. A. Kivelson, M. R. Norman, S. Uchida, and J. Zaanen, High temperature superconductivity in the cuprates, *Nature (London)* **518**, 179 (2015).
- [62] A. Georges, G. Kotliar, W. Krauth, and M. J. Rozenberg, Dynamical mean-field theory of strongly correlated fermion systems and the limit of infinite dimensions, *Rev. Mod. Phys.* **68**, 13 (1996).
- [63] J. Merino and R. H. McKenzie, Transport properties of strongly correlated metals: A dynamical mean-field approach, *Phys. Rev. B* **61**, 7996 (2000).
- [64] B. Kyung, S. S. Kancharla, D. Sénéchal, A.-M. S. Tremblay, M. Civelli, and G. Kotliar, Pseudogap induced by short-range spin correlations in a doped Mott insulator, *Phys. Rev. B* **73**, 165114 (2006).
- [65] G. Kotliar, S. Y. Savrasov, K. Haule, V. S. Oudovenko, O. Parcollet, and C. A. Marianetti, Electronic structure calculations with dynamical mean-field theory, *Rev. Mod. Phys.* **78**, 865 (2006).
- [66] D. Gotfryd, E. Pärschke, J. Chaloupka, A. M. Oleś, and K. Wohlfeld, How spin-orbital entanglement depends on the spin-orbit coupling in a Mott insulator, *Phys. Rev. Res.* **2**, 013353 (2020).
- [67] D. Gotfryd, E. Pärschke, K. Wohlfeld, and A. M. Oleś, Evolution of spin-orbital entanglement with increasing Ising spin-orbit coupling, *Condens. Matter* **5**, 53 (2020).
- [68] A. M. Oleś, Antiferromagnetism and correlation of electrons in transition metals, *Phys. Rev. B* **28**, 327 (1983).
- [69] A. B. Harris, T. Yildirim, A. Aharony, Ora Entin-Wohlman, and I. Y. Korenblit, Unusual Symmetries in the Kugel-Khomskii Hamiltonian, *Phys. Rev. Lett.* **91**, 087206 (2003).

- [70] M. Daghofer, K. Wohlfeld, A. M. Oleś, E. Arrighoni, and P. Horsch, Absence of Hole Confinement in Transition-Metal Oxides with Orbital Degeneracy, *Phys. Rev. Lett.* **100**, 066403 (2008).
- [71] K. Wohlfeld, M. Daghofer, A. M. Oleś, and P. Horsch, Spectral properties of orbital polarons in Mott insulators, *Phys. Rev. B* **78**, 214423 (2008).
- [72] P. Wróbel and A. M. Oleś, Ferro-Orbitally Ordered Stripes in Systems with Alternating Orbital Order, *Phys. Rev. Lett.* **104**, 206401 (2010).
- [73] P. Wróbel, R. Eder, and A. M. Oleś, Optical conductivity due to orbital polarons in systems with orbital degeneracy, *Phys. Rev. B* **86**, 064415 (2012).
- [74] P. Horsch, J. Jaklič, and F. Mack, Optical conductivity of colossal-magnetoresistance compounds: Role of orbital degeneracy in the ferromagnetic phase, *Phys. Rev. B* **59**, 6217 (1999).
- [75] F. Mack and P. Horsch, Optical Conductivity in Doped Manganites with Planar x^2-y^2 Orbital Order, *Phys. Rev. Lett.* **82**, 3160 (1999).
- [76] C. Zener, Interaction Between the d Shells in the Transition Metals, *Phys. Rev.* **81**, 440 (1951).
- [77] E. Dagotto, T. Hotta, and A. Moreo, Colossal magnetoresistant materials: The key role of phase separation, *Phys. Rep.* **344**, 1 (2001).
- [78] E. Dagotto, Open questions in CMR manganites, relevance of clustered states and analogies with other compounds including the cuprates, *New J. Phys.* **7**, 67 (2005).
- [79] T. V. Ramakrishnan, Modelling colossal magnetoresistance manganites, *J. Phys.: Condens. Matter* **19**, 125211 (2007).
- [80] Y. Tokura, Critical features of colossal magnetoresistive manganites, *Rep. Prog. Phys.* **69**, 797 (2006).
- [81] R. Kilian and G. Khaliullin, Orbital polarons in the metal-insulator transition of manganites, *Phys. Rev. B* **60**, 13458 (1999).
- [82] M. Daghofer, A. M. Oleś, and W. von der Linden, Orbital polarons versus itinerant e_g electrons in doped manganites, *Phys. Rev. B* **70**, 184430 (2004).
- [83] G. Khaliullin and R. Kilian, Theory of anomalous magnon softening in ferromagnetic manganites, *Phys. Rev. B* **61**, 3494 (2000).
- [84] A. M. Oleś and L. F. Feiner, Why spin excitations in metallic ferromagnetic manganites are isotropic, *Phys. Rev. B* **65**, 052414 (2002).
- [85] The sign convention taken here is natural for the purely electronic problem, and is opposite to that in [13] which is commonly used in the Jahn-Teller problem for e_g doublets; cf. R. Englman, *The Jahn-Teller Effect in Molecules and Crystals* (John Wiley, London, 1972).
- [86] J. R. Klauder, Path integrals and stationary-phase approximations, *Phys. Rev. D* **19**, 2349 (1979).
- [87] Note that θ_i is the azimuthal, not the polar angle.
- [88] N. C. Petroni, *Probability and Stochastic Processes for Physicists* (Springer, Berlin, 2021).
- [89] J. Bünemann, W. Weber, and F. Gebhard, Multiband Gutzwiller wave functions for general on-site interactions, *Phys. Rev. B* **57**, 6896 (1998).
- [90] E. W. Ng and M. Geller, A table of integrals of the error functions, *J. Res. NBS B Math. Sci.* **73B**, 1 (1969).
- [91] W. F. Brinkman and T. M. Rice, Application of Gutzwiller's variational method to the metal-insulator transition, *Phys. Rev. B* **2**, 4302 (1970).
- [92] This is an idealization and at finite dimension the condition $d = 0$ is satisfied only at $U = \infty$, because the Brinkman-Rice criterion neglects virtual excitations, which generate antiferromagnetism at finite U in the spin Hubbard model.
- [93] P. G. J. van Dongen, F. Gebhard, and D. Vollhardt, Variational evaluation of correlation functions for lattice electrons in high dimensions, *Z. Phys. B* **76**, 199 (1989).
- [94] D. Vollhardt, Dynamical Mean-Field Approach for Strongly Correlated Materials, in *Lecture Notes of the Autumn School on Correlated Electrons 2011*, Vol. 1, edited by E. Pavarini, E. Koch, D. Vollhardt, and A. Lichtenstein (Verlag des Forschungszentrum Jülich, Jülich, 2011).
- [95] D. Vollhardt, From Gutzwiller Wave Function to Dynamical Mean-Field Theory, in *Lecture Notes of the Autumn School on Correlated Electrons 2014*, Vol. 4, edited by E. Pavarini, E. Koch, D. Vollhardt, and A. Lichtenstein (Verlag des Forschungszentrum Jülich, Jülich, 2014).
- [96] D. Vollhardt, From Infinite Dimensions to Real Materials, in *Lecture Notes of the Autumn School on Correlated Electrons 2018*, Vol. 8, edited by E. Pavarini, E. Koch, A. Lichtenstein, and D. Vollhardt (Verlag des Forschungszentrum Jülich, Jülich, 2018).
- [97] G. Kotliar, Electronic Structure of Correlated Materials: Slave-Boson Methods and Dynamical Mean-Field Theory, in *Lecture Notes of the Autumn School on Correlated Electrons 2018*, Vol. 8, edited by E. Pavarini, E. Koch, A. Lichtenstein, and D. Vollhardt (Verlag des Forschungszentrum Jülich, Jülich, 2018).
- [98] J. K. Freericks and V. Zlatić, Exact dynamical mean-field theory of the Falicov-Kimball model, *Rev. Mod. Phys.* **75**, 1333 (2003).
- [99] H. Aoki, N. Tsuji, M. Eckstein, M. Kollar, T. Oka, and P. Werner, Nonequilibrium dynamical mean-field theory and its applications, *Rev. Mod. Phys.* **86**, 779 (2014).
- [100] L. de' Medici, A. Georges, and S. Biermann, Orbital-selective Mott transition in multiband systems: Slave-spin representation and dynamical mean-field theory, *Phys. Rev. B* **72**, 205124 (2005).
- [101] E. Jakobi, N. Blümer, and P. van Dongen, Orbital-selective Mott transitions in a doped two-band Hubbard model with crystal field splitting, *Phys. Rev. B* **87**, 205135 (2013).
- [102] M. Kollar and D. Vollhardt, Exact analytic results for the Gutzwiller wave function with finite magnetization, *Phys. Rev. B* **65**, 155121 (2002).
- [103] R. Frésard and G. Kotliar, Interplay of Mott transition and ferromagnetism in the orbitally degenerate Hubbard model, *Phys. Rev. B* **56**, 12909 (1997).
- [104] T. Obermeier, T. Pruschke, and J. Keller, Ferromagnetism in the large- U Hubbard model, *Phys. Rev. B* **56**, R8479 (1997).
- [105] P. Fazekas, *Lecture Notes on Electron Correlation and Magnetism* (World Scientific, Singapore, 1999).
- [106] R. Bulla, Zero Temperature Metal-Insulator Transition in the Infinite-Dimensional Hubbard Model, *Phys. Rev. Lett.* **83**, 136 (1999).

- [107] M. J. Rozenberg, R. Chitra, and G. Kotliar, Finite Temperature Mott Transition in the Hubbard Model in Infinite Dimensions, *Phys. Rev. Lett.* **83**, 3498 (1999).
- [108] R. Bulla, T. A. Costi, and D. Vollhardt, Finite-temperature numerical renormalization group study of the Mott transition, *Phys. Rev. B* **64**, 045103 (2001).
- [109] E. G. C. P. van Loon, F. Krien, and A. A. Katanin, Bethe-Salpeter Equation at the Critical End Point of the Mott Transition, *Phys. Rev. Lett.* **125**, 136402 (2020).
- [110] K. I. Kugel, D. I. Khomskii, A. O. Sboychakov, and S. V. Streltsov, Spin-orbital interaction for face-sharing octahedra: Realization of a highly symmetric SU(4) model, *Phys. Rev. B* **91**, 155125 (2015).
- [111] V. E. Valiulin, A. V. Mikheyenkov, K. I. Kugel, and A. V. Barabanov, Thermodynamics of symmetric spin-orbital model: One- and two-dimensional cases, *JETP Lett.* **109**, 546 (2019).
- [112] N. J. Laurita, J. Deisenhofer, L.-D. Pan, C. M. Morris, M. Schmidt, M. Johnsson, V. Tsurkan, A. Loidl, and N. P. Armitage, Singlet-Triplet Excitations and Long-Range Entanglement in the Spin-Orbital Liquid Candidate FeSc₂S₄, *Phys. Rev. Lett.* **114**, 207201 (2015).
- [113] H. Takagi, T. Takayama, G. Jackeli, G. Khaliullin, and S. E. Nagler, Kitaev quantum spin liquid—concept and materialization, *Nat. Rev. Phys.* **1**, 264 (2019).
- [114] J. Bünemann, K. Jávorné-Radnóczy, P. Fazekas, and F. Gebhard, Orbital order in degenerate Hubbard models: A variational study, *J. Phys.: Condens. Matter* **19**, 326217 (2007).
- [115] Y. Nagaoka, Ferromagnetism in a Narrow, Almost Half-Filled s Band, *Phys. Rev.* **147**, 392 (1966).
- [116] J. van den Brink and D. Khomskii, Orbital ordering of complex orbitals in doped Mott insulators, *Phys. Rev. B* **63**, 140416(R) (2001).
- [117] <https://www.humboldt-foundation.de/web/humboldt-preis.html>